

Air–sea exchanges in the equatorial area from the EQUALANT99 dataset: Bulk parametrizations of turbulent fluxes corrected for airflow distortion

By A. BRUT†, A. BUTET, P. DURAND, G. CANIAUX and S. PLANTON
CNRM‡, Météo France, Toulouse Cedex, France

(Received 24 September 2003; revised 7 March 2005)

SUMMARY

Turbulent fluxes of momentum, sensible heat and water vapour were calculated using both the eddy covariance (EC) and the inertial dissipation (ID) methods applied to data collected on board the research vessel *La Thalassa* during 40 days of the EQUALANT99 oceanographic campaign. The aim of this experiment was to establish accurate parametrizations of air–sea fluxes for the equatorial Atlantic area from a large dataset. However, the accuracy of turbulent fluxes measured aboard ships is strongly affected by the distortion of airflow patterns generated by obstacles such as the ship and mast. For the EQUALANT99 experiment, the effects of airflow distortion were estimated using physical simulations in a water channel. To reproduce the conditions of the campaign, a neutral boundary layer was simulated in the water channel and a detailed model of the ship *La Thalassa* was built. Correction coefficients for the mean wind speed were evaluated from these physical simulations. They show a dependence on both the azimuth angle of the flow (i.e. the horizontal direction of the flow with respect to the ship's longitudinal axis) and the angle of incidence of the wind. The correction for airflow distortion was applied to the measured wind speed and also included in the flux computation using the ID method. Compared with earlier studies which applied a single correction per flux sample, it appears that our results for the corrected transfer coefficients present greater dependence on neutral wind speed than the previous parametrizations; the method also shows encouraging results, with a decrease in the scatter of the transfer coefficients parametrization. However, the distortion could not be corrected for in the fluxes calculated using the EC method, because this technique integrates a wide range of turbulence scales for which the airflow distortion cannot be simulated in a water channel.

Fluxes computed using the ID and EC methods are presented and compared in order to determine which method, in the configuration of the EQUALANT99 experiment, provides the best resulting transfer coefficients. According to the results, fluxes of momentum and latent heat computed by ID were better for deriving the drag and humidity coefficients. The EC method seemed better adapted to calculate sensible-heat fluxes than the ID method, although a high scatter remained on the Stanton neutral number.

KEYWORDS: Air–sea flux measurements Eddy correlation Inertial dissipation method Open ocean

1. INTRODUCTION

Turbulent fluxes of momentum, sensible and latent heat are involved in many aspects of meteorological and oceanographical research (e.g. climate studies, weather forecasting, modelling of boundary-layer processes etc.). The turbulent exchanges between ocean surfaces and the atmosphere are particularly important given that oceans cover a large part of the earth's surface. These interactions widely control the large-scale atmospheric circulation patterns and the ocean dynamics. At smaller scales, they also affect mixed-layer development and wave generation. Sea-surface exchanges may considerably influence violent cyclogenesis and cloud organization through evaporation processes (see for example the CATCH and FASTEX experiments, Eymard *et al.* (1999) and Joly *et al.* (1997)). Thus, accurate estimations of turbulent surface fluxes are essential for the quantification of ocean–atmosphere coupling mechanisms and to evaluate the role of the ocean in weather and climate variability.

In numerical modelling exercises, air–sea fluxes are quantified through parametrizations (bulk fluxes) related to the mean meteorological variables. But for each of these fluxes (momentum, sensible and latent heat) the parametrizations derived from direct

† Corresponding author: Météo France, CNRM/URA CNRS 1357, 42 Avenue Coriolis, 31057 Toulouse Cedex, France. e-mail: aurore.brut@cnrm.meteo.fr

‡ Centre National de Recherches Météorologiques.

© Royal Meteorological Society, 2005.

measurements differ from one experiment to another (Smith *et al.* 1996; Weill *et al.* 2003). Calculation methods, sea state, atmospheric stability conditions, airflow distortion and instrumental errors are all possible causes invoked to explain such differences (Geernaert 1990). For example, the difficulty of measuring fluxes over the sea due to the contamination of instruments by salt particles and spray has been investigated by Schacher and Fairall (1976), Schmitt *et al.* (1978), Larsen and Gibson (1980) and Larson *et al.* (1993). The choice of flux computation method also affects estimates of air–sea exchanges. The eddy-covariance (EC) technique consists of the direct measurement of the desired time-averaged covariance at the measurement height, but requires corrections for platform motion when used on board research vessels (RVs; Fujitani 1981; Edson *et al.* 1998; Pedreros *et al.* 2003). These authors showed that the fluxes (especially the momentum flux) were very sensitive to the accuracy of corrections applied for these motions. On the other hand, the inertial-dissipation (ID) method relies on measurements at high frequencies which are less affected by platform motion, but it also relies on assumptions necessary to solve the variance budgets equations. Despite its advantages, questions are raised concerning this method over the accuracy of empirical similarity functions and various constants, and the validity of approximations concerning the variance budget (Fairall and Larsen 1986; Edson *et al.* 1991; Yelland *et al.* 1994; Edson and Fairall 1998; Taylor and Yelland 2000). For instance, the theory which supports the ID method was developed under the assumption of locally isotropic turbulence and, therefore, the dissipation technique has long been criticized as lacking justification in a boundary-layer shear flow. Henjes (1998) studied the impact of the method when applied to explicitly anisotropic conditions, and recommended that the block lengths should not exceed the order of the eddy lifetime in the computation of the spectra.

Another problem to be addressed when studying the air–sea fluxes is the effect of the sea-state and wave age on the wind stress. The ocean surface is not flat and cannot be represented as a constant roughness, but consists of waves that interact with the atmosphere. Using dimensional arguments, Charnock (1955) proposed a link between the roughness length, z_0 , and friction velocity, u_* , via a dimensionless constant α . However, this ‘constant’ was found to depend on the measurement location. Donelan *et al.* (1993) modified the study by proposing relationships between the drag coefficient and a ‘wave-age’ parameter $\xi = c_{\text{peak}} u_*^{-1}$, where c_{peak} is the phase velocity of the peak of the wave spectrum. Conclusions from various studies are that, for a given wind speed, the drag coefficient will be larger in the presence of recent or underdeveloped waves. For instance, Volkov (1970) and Donelan *et al.* (1997) noticed that the presence of strong swell can modify the momentum flux over typical open-ocean values. Studies from Drennan *et al.* (2003) found similar results for developing wind-waves. Furthermore, Anctil and Donelan (1994) and Oost (1998) have shown that shoaling waves can lead to a modified drag relation, with the surface roughness enhanced by wave breaking. However, doubts still remain about the applicability of the relationships found, since they vary greatly from one experiment to another (see review by Komen *et al.* 1998).

Although developments in instrumentation have enabled significant improvements in flux measurements, such measurements remain a considerable challenge over ocean surfaces. Among the difficulties lies the problem of flow distortion caused by ship structures and masts (Blanc 1986, 1987; Oost *et al.* 1994). Previous studies have used numerical simulations to evaluate the corrections for airflow distortion. For instance, Yelland *et al.* (1998) estimated wind speed corrections using code VECTIS of Computational Fluid Dynamics (CFD). They observed that the changes in the relative wind direction strongly affect the airflow distortion, and they found that the neutral drag coefficient was reduced by a minimum of 6% for bow-on winds over the RV *Discovery* when corrections

for airflow distortion were applied. For the RV *Charles Darwin*, they showed that the impact of a mean correction was about 40% for the drag coefficient and they found larger values for bow-off flows. A further study pointed out that the airflow vertical displacement, induced by distortion, also depends on the wind azimuth angle. Corrections for this effect are found to modify the drag coefficient as much as the wind speed correction (Yelland *et al.* 2002), but the impact of the airflow lift on corrections strongly depends on the ship geometry (sensors and mast location). Dupuis *et al.* (2003) also used numerical simulations of airflow distortion (codes FLUENT and CFD) to estimate corrections for the flux-transfer coefficients. Following the method proposed by Yelland *et al.* (1998), these authors applied corrections for airflow distortion to the mean wind speed and to fluxes computed by the ID method. Their corrections led to a decrease in the neutral drag coefficient, C_{Dn} , and a reduction of scatter in the data; the same was found for the exchange coefficient for evaporation, C_{En} .

This paper seeks to provide a thorough study of air-sea exchanges from the significant dataset of the EQUALANT99 campaign (Gouriou *et al.* 2001). This experiment is part of the ALBATROS (AUTOFLUX Linked Base for Atmospheric TRansfer at the Ocean Surface) database. This latter gathers measurements performed onboard RVs during various experimental campaigns from 1992 to 2001; it is devoted to air-sea exchanges and was initiated by the French community (Weill *et al.* 2003). It includes data from the following experiments: SOFIA/ASTEX (Weill *et al.* 1995), SEMAPHORE (Eymard *et al.* 1996), CATCH/FASTEX (Eymard *et al.* 1999), FETCH (Hauser *et al.* 2003), EQUALANT99, and POMME (Memery *et al.* 2005). ALBATROS has been developed in the framework of AUTOFLUX (<http://dataserv.cep.ipsl.fr/FLUX/>) which is a European programme for the measurement and parametrization of air-sea fluxes, aimed at the standardization of instrumental packages, data processing and flux-computation algorithms (Larsen *et al.* 2000). The database yields extensive datasets of turbulent and mean meteorological parameters, collected during a large diversity of weather and oceanic situations, for the international community. Subsequently, the large amount of data has made it possible to initiate new studies and develop standard methods to improve estimates of air-sea fluxes.

During EQUALANT99, the instrumental set up implemented onboard the RV *La Thalassa* enabled the computation of fluxes using both ID and EC methods. Advantages and drawbacks of both techniques are summed up in this paper using a comparison of turbulent fluxes computed by both methods. We focus mainly on the fluxes of momentum and latent heat, due to the high-frequency noise observed in data provided by the sonic thermometer. Our objective is the determination of accurate bulk parametrizations taking account of airflow distortion corrections. Since the EC technique cannot be corrected for airflow distortion, corrections are only applied to the ID momentum and latent-heat fluxes. In the present study the effect of airflow distortion is estimated using physical simulations in a water channel; several experimental configurations allow us to determine correction coefficients for the mean wind speed according to the wind azimuth angle, and to the angle of wind incidence which depends on the pitch angle (Butet 2001). From this preliminary study, a new methodology is used to correct the wind velocity at the frequency of 1 Hz; this is an original approach, and compares with the previous method of applying a single correction per flux estimate.

The paper is presented as follows: in section 2 we describe the objectives, the experimental set-up and the meteorological conditions of the EQUALANT99 experiment; a brief review of the theory of flux computation methods is also included in this section. Then, in section 3 the main results obtained from physical simulations in the water tank are presented, the methodology to apply corrections for airflow distortion is

explained, and the consistency of the airflow correction is evaluated for the ID method. In section 4, EC and ID flux computation methods are discussed, and comparisons of turbulent fluxes computed by three methods (EC, ID and bulk) are presented. In the final section an updated bulk parametrization of turbulent air–sea fluxes is proposed.

2. THE EQUALANT99 EXPERIMENT AND DATA PROCESSING

(a) Description of EQUALANT99

The EQUALANT99 project (<http://nansen.ipsl.jussieu.fr/EQUALANT/>) was part of an oceanographic programme led by the IRD (the French Institut de Recherches pour le Développement) for the study of deep oceanic circulations in the Equatorial Atlantic basin (Gouriou *et al.* 2001). The cruise of RV *La Thalassa* took place between Salvador de Bahia (Brazil) and Abidjan (Ivory Coast) during the summer months of 1999. This intertropical area, which receives most solar radiation, plays a major role in the earth's climate. However, large uncertainties remain concerning the characteristics of the surface energy balance. This region is also characterized by the equatorial upwelling which also directly affects the transport of heat energy. The main focus of the EQUALANT99 experiment was to develop a parametrization for turbulent fluxes, which is urgently needed in this region for the PIRATA programme (Servain *et al.* 1998) which deals with the monitoring of the ocean surface using the network of ATLAS moored buoys. In Fig. 1 the mooring network is represented along with the ship's trajectory, which consists of three transects orientated north–south. Time series of mean meteorological parameters encountered during this experiment are plotted in Figs. 2 and 3. From Fig. 2 we observe that the dataset was mainly collected during sustained south-easterly winds (trade winds) ranging from 2 to 13 m s⁻¹. In addition, atmospheric conditions showed weak unstable stratifications for most of the campaign, but at the end of the cruise conditions became stable as a result of lower sea surface temperature in an area of coastal upwelling (Fig. 3). With the exception of the eastern boundary of the basin, air masses are 1 or 2 degC cooler than the ocean surface in the equatorial Atlantic area. Mean sea temperature varies between 23 °C near the eastern coast to more than 28 °C in the western Atlantic ocean. Sensible-heat fluxes are very sensitive to this parameter, as they are computed using the wind speed and the temperature difference between the sea and the atmosphere. Thus, a small error in the sea temperature measurement results in large errors in bulk heat-flux calculation.

(b) Experimental set-up

Two types of measurements were carried out during EQUALANT99. The location of the mast instruments can be seen on Figs. 4 and 5. Turbulent signals of the three wind components, and the 'sonic' temperature were recorded using an ultrasonic anemometer (R3 research HS, from Gill Instruments Ltd.) at a frequency rate of 50 Hz. In addition, a microwave refractometer (Delahaye *et al.* 2001) measured the atmospheric refraction index, n , from its 9 GHz resonant cavity. Hence, the specific humidity q (g kg⁻¹), and air temperature T (K) as well as their fluctuations could be derived from the sonic temperature T_s (K) and refractive-index signals through empirical relations. According to Delahaye *et al.* (2001), the microwave refractivity, N , is expressed as: $N = 10^6(n - 1) = p\{(77.6/T) + (3.73 \times 10^5 q / 0.622T^2)\}$, where p is the air pressure (hPa).

In addition, T is related to T_s by the formula: $T_s = T(1 + 0.518 \times 10^{-3}q)$ (Kaimal and Gaynor 1991).

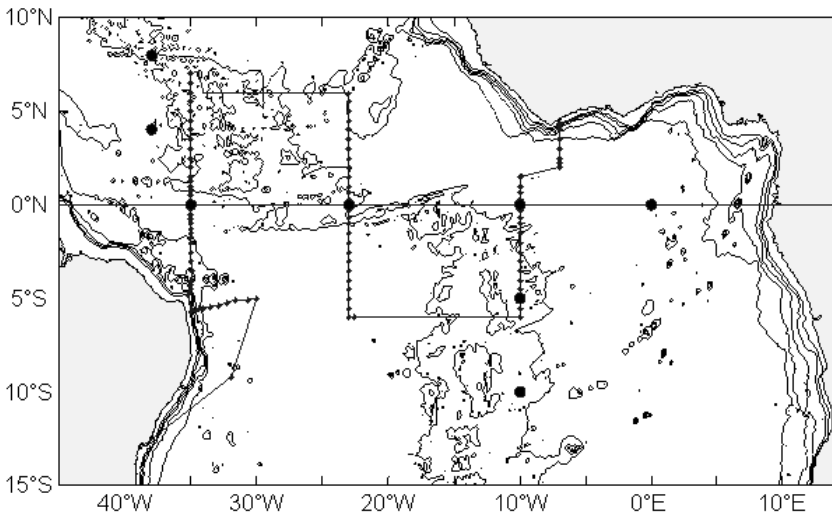


Figure 1. Route of RV *La Thalassa* in the equatorial Atlantic ocean during the EQUALANT99 experiment from 14 July to 22 August 1999. The small dots along the trajectory correspond to fixed measurement points. The large dots correspond to the PIRATA buoy arrays.

These two formulae involve two unknowns (T and q) since the only measured parameters are the sonic temperature and the refraction index. This system leads to polynomial equations for T and q which are solved using numerical methods.

In order to compute the EC fluxes, a motion package (TSS 335B from TSS Inc.) documented the ship movements (pitch, roll and heave) at the same frequency as for the flow velocities. The heave was obtained by performing a double integration of the linear accelerometer signal. This signal is then filtered after each integration in order to limit the low-frequency response of the system and to minimize the error from random noise. The filtering is carried out automatically and instantaneously by the motion package processing algorithm. Navigation parameters were also recorded on board the ship, at frequency rates of 1 and 0.1 Hz: the gyrocompass and electromagnetic log collected the true heading and ship velocity signals, respectively. Unlike Zeller *et al.* (2001) who used an analogue-to-digital 'datapacker' system with their sonic anemometer and LiCor sensor, we opted to acquire the signals of the motion package and the refractometer through the analogue input of the sonic anemometer. This allows us to reduce the time lag between the various parameters. In our case, no delay was observed between the motion package and the sonic anemometer signals, whereas Zeller *et al.* (2001) reported a loss in the magnitude of the measured flux due to a systematic microprocessor-caused lag in their independent datapacker system.

In addition, the fast computer clock regularly triggered the recording of data from the anemometer output and allowed their precise timing. The possible lag between data can arise from 'undersampling' of the ship's navigation parameters (ship speed and heading) and the high-frequency data collected from the mast sensors. Actually, the navigation parameters were acquired from the ship's own system and were timed using the ship's clock. A post-synchronization of the navigation parameters with the sonic anemometer signals was intended, although their acquisition frequencies were different (1 Hz for heading, 0.1 Hz for ship velocity and 50 Hz for other signals), so delays of a few seconds may exist on heading and ship velocity signals which limits the full correction of the horizontal wind velocities to compensate for the ship motions.

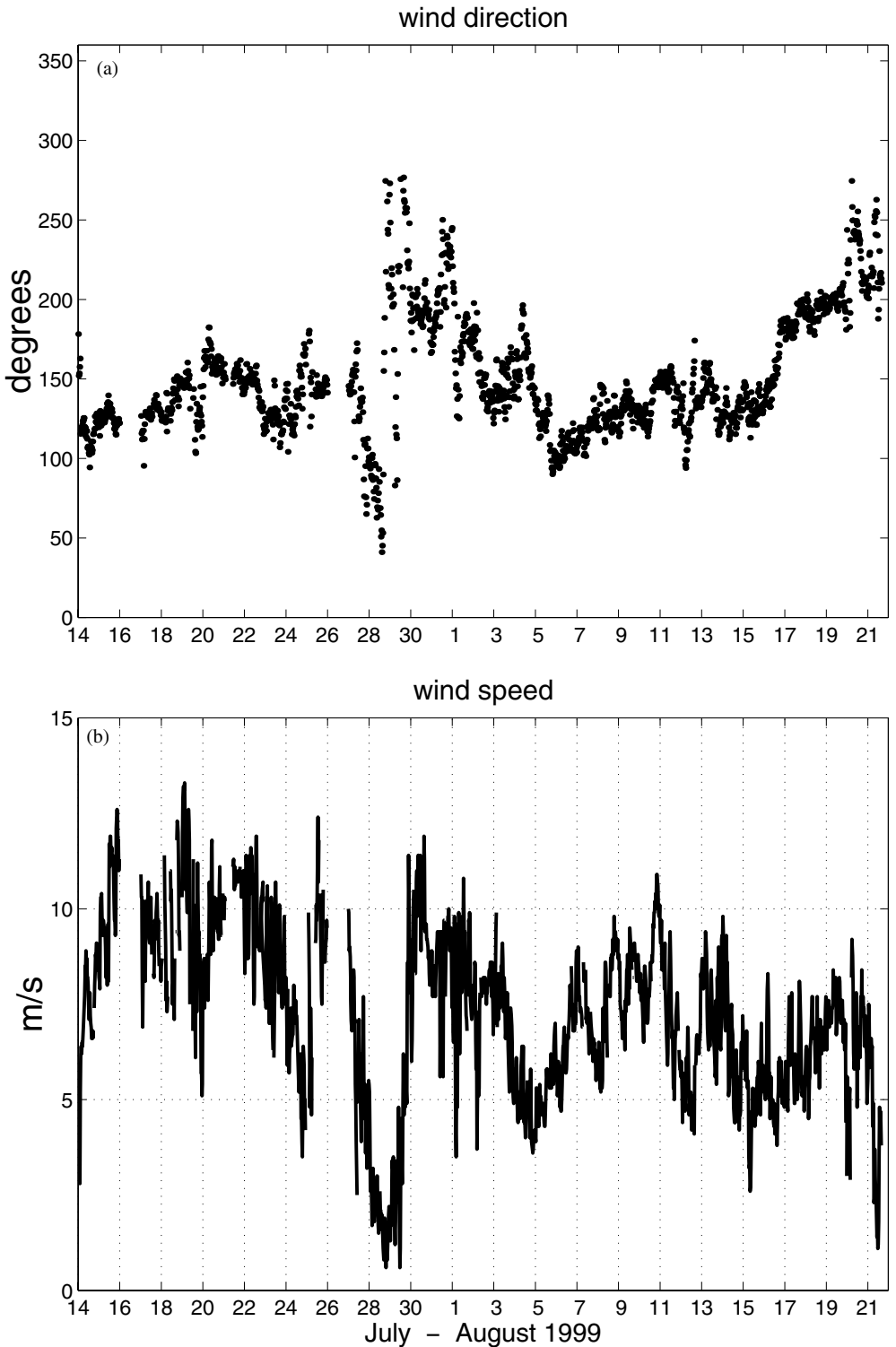


Figure 2. Time series of: (a) wind direction, and (b) wind strength along the route of RV *La Thalassa* during the EQUALANT99 experiment from 14 July to 22 August 1999.

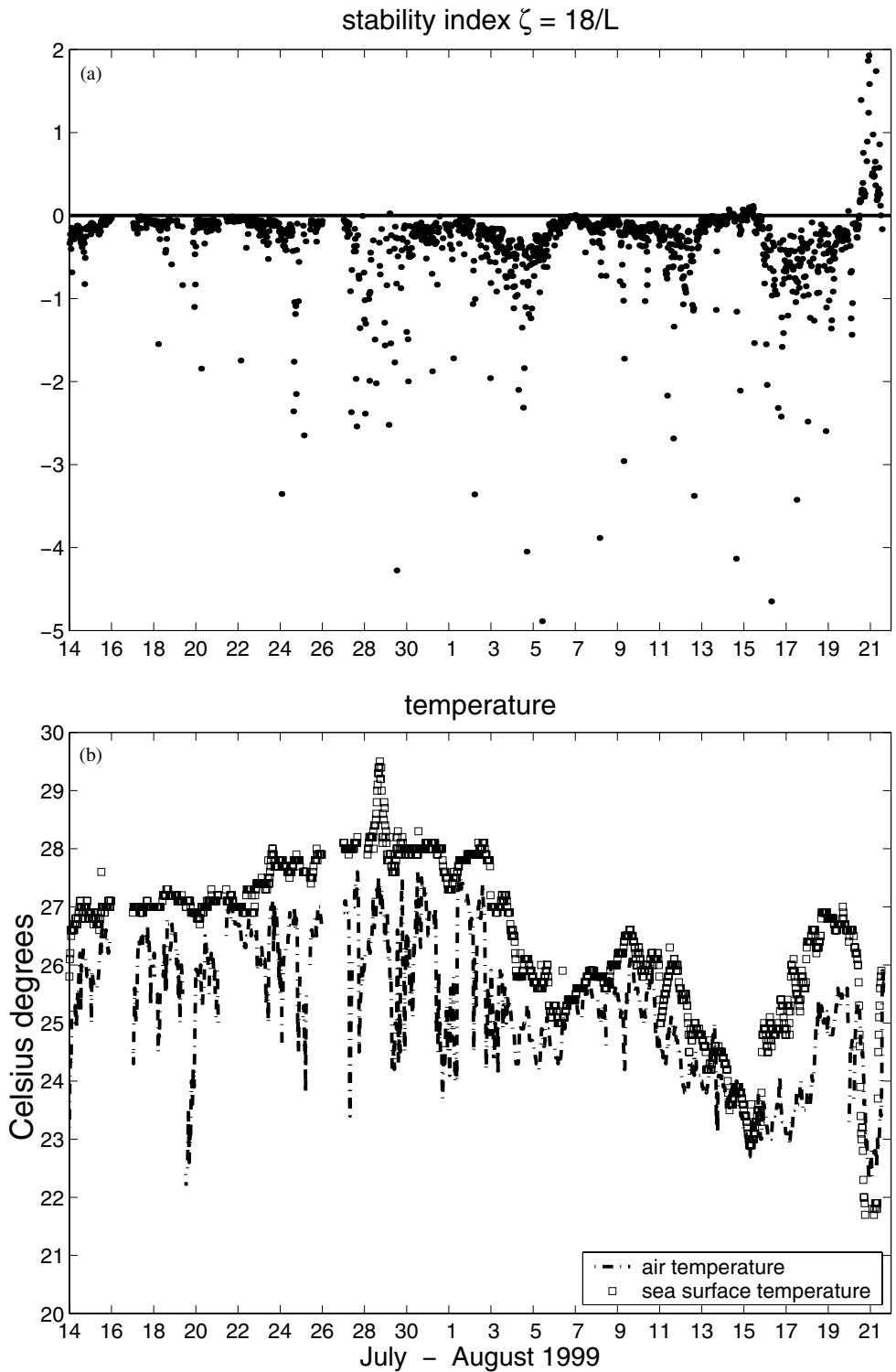
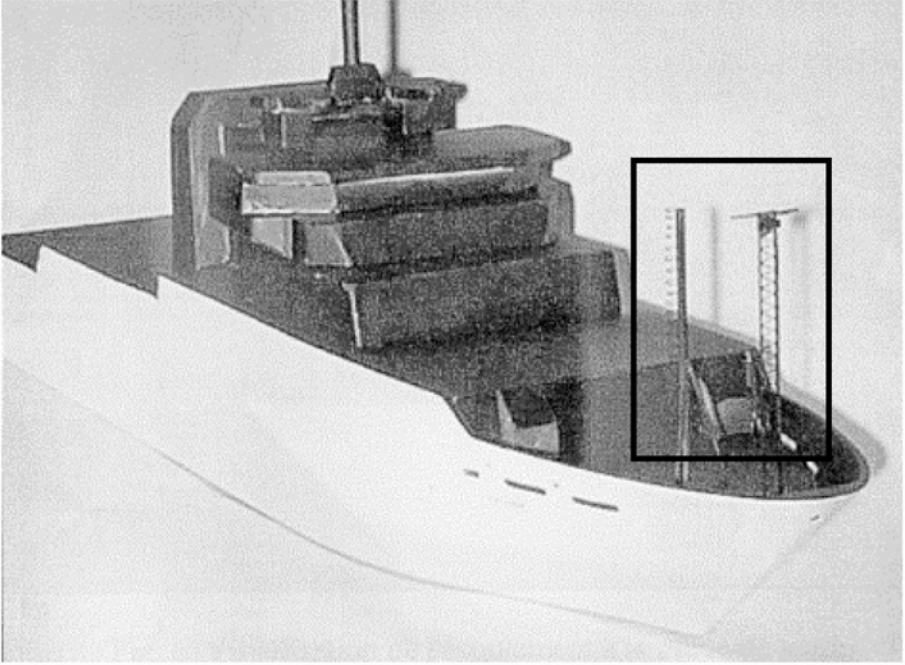


Figure 3. Time series of: (a) the stability index computed 18 m above the sea surface, and (b) air temperature (dashed line) and sea temperature (squares) measured along the route of RV *La Thalassa* during the EQUALANT99 experiment from 14 July to 22 August 1999.

(a)



(b)



(c)

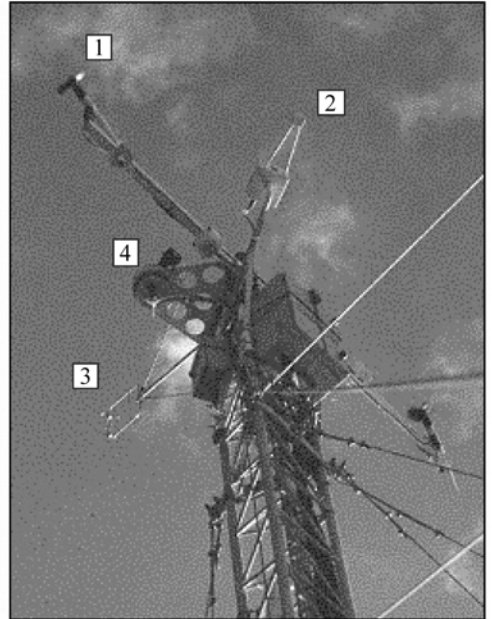


Figure 4. (a) Model of the RV *La Thalassa* (1/60 scale) used for the simulation in the water channel at Centre National de Recherches Météorologiques, Météo France; (b) details of the real ship's mast, as modelled in the rectangular frame in (a). (c) At the top of the mast: 1 corresponds to sensors measuring the mean meteorological data, 2 is the rain optical sensor, 3 is the 3-D sonic anemometer and 4 is the microwave refractometer.

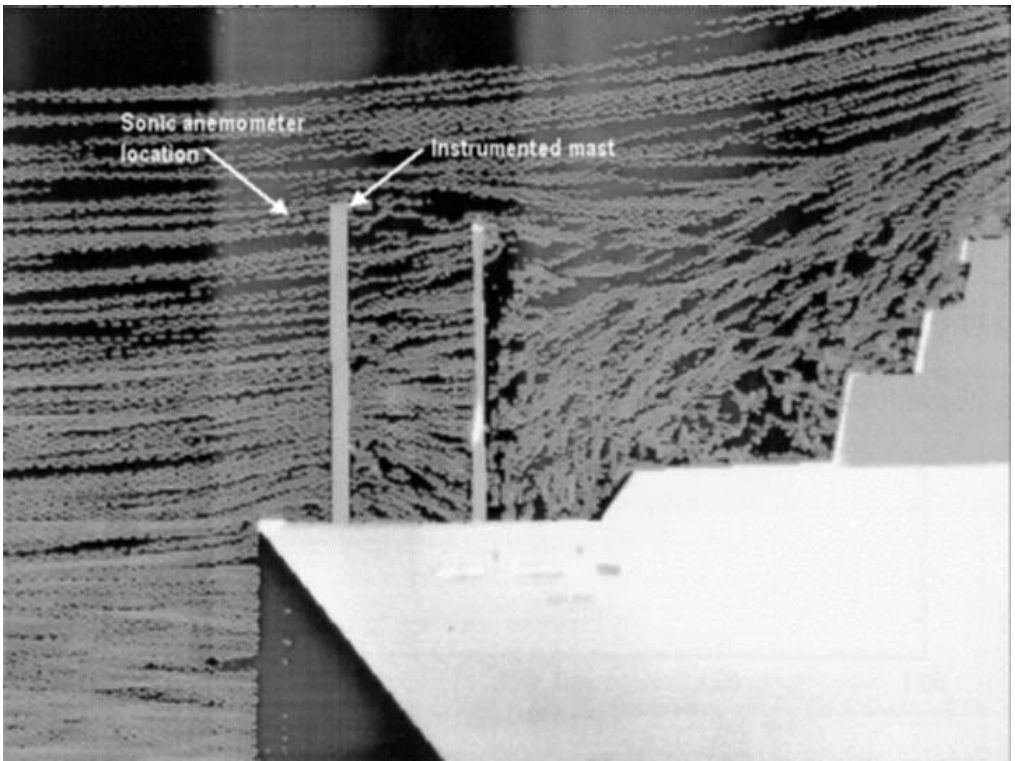


Figure 5. Example of picture obtained by laser tomography of particles in the water flowing past the model (1/60 scale) of the RV *La Thalassa* in the water channel. This enables visualization of the airflow distortion around the masts and superstructure of the real vessel. The parcel trajectories are represented by white lines.

Furthermore, the spatial layout of the sonic anemometer and the refractometer can affect the estimation of latent-heat fluxes computed by the EC method (Kristensen *et al.* 1997). Both instruments were located about 18 m above the sea surface, on an 11 m high mast installed on the foredeck of the ship, but the acoustic transmitters and receivers of the sonic anemometer were displaced 80 cm in front of the mast axis (see Fig. 5). Thus there is a delay between data due to the distance between sensors. The signal for the air refraction index had, therefore, to be shifted by a time equal to the sensors separation of 0.8 m divided by the horizontal relative mean wind U_r for bow-on flow conditions.

Most of the sensors for the mean meteorological measurements were also mounted on top of the mast. Two symmetrical probes (model HMP353 from Väisälä), located on each side of the mast, yielded mean values of air temperature and humidity. Atmospheric pressure was measured using a Väisälä PTB220 barometer. Two wind sensors (YOUNG model 05305) measured mean direction and speed of the relative wind from each side of the mast. We chose to use the bulk sea temperature instead of the sea-surface temperature, and it was measured by a thermo-salinograph Seabird SBE-21. The sea-water intake was located under the ship's hull near the bow, at a depth of 5 m below the sea surface. Its sampling rate during the cruise was 0.1 Hz and its measurement range varies from -5 to 35 °C with an accuracy of 0.05 degC. Table 1 summarizes instrument specifications as well as any pre- or post-cruise calibrations.

TABLE 1. SPECIFICATIONS OF THE TURBULENCE AND NAVIGATION SENSORS IMPLEMENTED ON BOARD RV *La Thalassa* DURING EQUALANT99

Parameter	Sensors	Frequency (Hz)	Instrument accuracy	Calibration
Sonic temperature	Sonic thermometer R3 Gill Ltd.	50	0.01 degC (0 to 50 °C)	Pre-cruise
Wind speed components	Sonic anemometer R3 Gill Ltd.	50	1% r.m.s.	Pre-cruise
Air refraction index	Refractometer	50	$\pm 2 \times 10^{-6}$ for the measurement of the air refractive index 5 cm or 5% whichever is the greater	Pre-and post-cruise
Heave	Motion package TSS 335B	50		Post-cruise
Roll	Motion package TSS 335B	50		
Pitch	Motion package TSS 335B	50	0.1°	
Ship speed	Electromagnetic log	1.0	0.1 knots up to 10 knots—1% full scale	—
Ship heading	Gyrocompass	0.1	0.2°	—
Sea temperature	Thermo-salinograph	0.1	0.05 degC	—

(c) *Flux computation algorithms*

In this section, we describe the data processing operated in the EC and ID algorithms.

(i) *Eddy covariance technique.* The EC method computes the covariances of the fluctuations of the vertical wind and of physical parameters of interest (horizontal wind components, temperature and specific humidity). When used on mobile platforms, this technique requires corrections to be made to the measured wind components so as to take ship movements into consideration. Previously, this method was performed on board ships and buoys as reported by, for example, Fujitani (1981), Dugan *et al.* (1991), Ancil *et al.* (1994) and Edson *et al.* (1998). In our processing algorithm, the ‘true’ wind vector \mathbf{V}_{cor} was derived using the approach proposed by Fujitani (1981):

$$\mathbf{V}_{\text{cor}} = \mathbf{T}\mathbf{V}_{\text{mes}} + \boldsymbol{\Omega} \wedge \mathbf{T}\mathbf{M} + \mathbf{V}_{\text{ship}}, \quad (1)$$

where \mathbf{V}_{mes} is the measured wind vector provided by the sonic anemometer, \mathbf{T} is the coordinate transformation matrix for a rotation of the platform frame coordinate system relative to the reference coordinate system, $\boldsymbol{\Omega}$ is the angular velocity vector of the platform coordinate system, \mathbf{V}_{ship} is the ship velocity vector, and \mathbf{M} is the vector distance between the locations of \mathbf{V}_{mes} and \mathbf{V}_{ship} measurements. \mathbf{V}_{ship} corresponds to the ship translatory movement and it is measured near the centre of gravity of the RV. The motion of a mobile point depends on six parameters: three rotation angles and three velocities for the translatory motion. However, the motion package which was located close to the sonic anemometer, only records two angles (pitch θ and roll φ) and the vertical position (heave, H). The gyrocompass yields the heading angle ψ (at 1 Hz frequency), however, since the log only provides a mean value of the ship velocity, it still lacks the high temporal resolution horizontal velocities necessary to accurately correct the measured wind velocities.

Here, the sign convention we adopt for the ship’s motion is as follows: x positive forward (to the bow), y positive to port, z positive upward, and ψ positive for the ship’s bow yawed clockwise from the north. The roll and pitch angles were recorded in the following unusual convention: φ is positive for the port side rolled up and θ positive for the bow pitched up. So, the corrected components of wind velocity (u , v , w) in the earth coordinate frame are derived using the following equations:

$$\begin{aligned} u = & \sin \psi \cos \theta (u_s - h\dot{\theta} + V_l) \\ & - (\sin \theta \sin \varphi \sin \psi + \cos \psi \cos \varphi) (v_s - l\dot{\psi} - h\dot{\varphi} - V_t) \\ & + (\sin \varphi \cos \psi - \sin \theta \sin \psi \cos \varphi) (w_s + l\dot{\theta}), \end{aligned} \quad (2)$$

$$\begin{aligned} v = & \cos \psi \cos \theta (u_s - h\dot{\theta} + V_l) \\ & + (-\sin \theta \sin \varphi \cos \psi + \cos \psi \sin \varphi) (v_s - l\dot{\psi} - h\dot{\varphi} - V_t) \\ & - (\sin \varphi \sin \psi + \sin \theta \cos \psi \cos \varphi) (w_s + l\dot{\theta}), \end{aligned} \quad (3)$$

$$w = \sin \theta u_s + \cos \theta \sin \varphi v_s + \cos \theta \cos \varphi w_s + H \quad (4)$$

where u_s , v_s , w_s , are the measured wind components in the sonic-anemometer frame, l and h are the longitudinal and vertical components of \mathbf{M} , respectively ($h = 18$ m, $l = 30$ m), in the ship-frame system: $x > 0$ forwards, $y > 0$ to starboard and $z > 0$ downwards, and V_l and V_t are the longitudinal and transverse components of the ship velocities in the ship-frame system, respectively. Signals at a frequency rate of 10 Hz

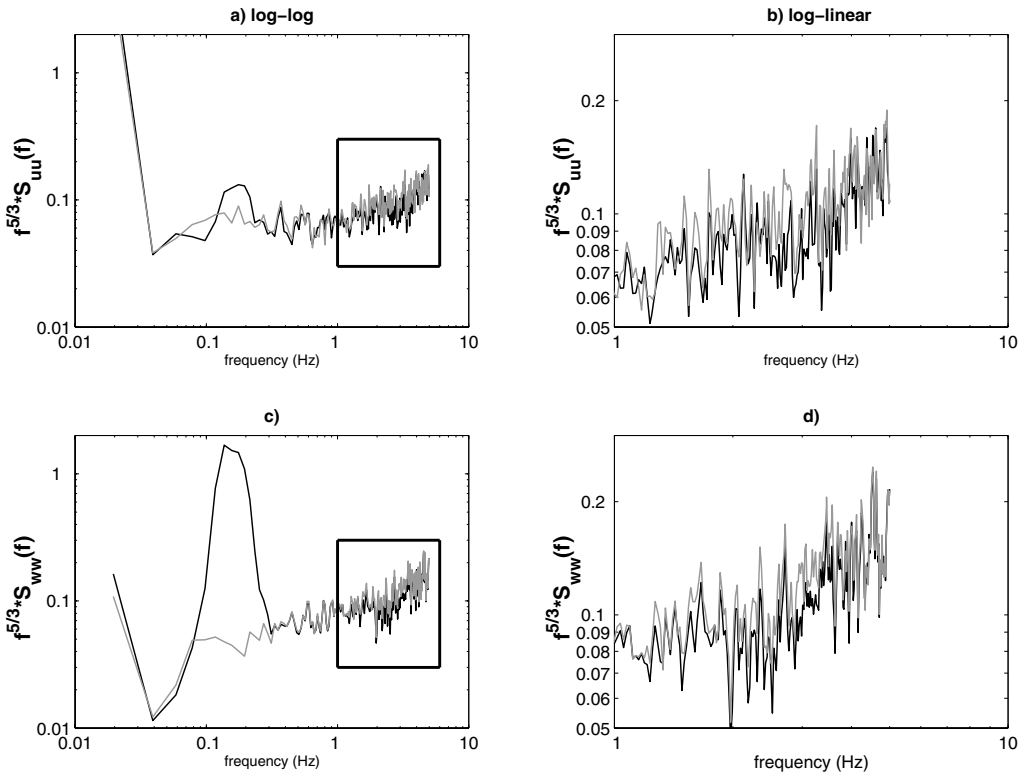


Figure 6. Examples of typical spectra of: (a) the longitudinal wind components computed from a 30-minute time series in logarithmic representation; (b) as (a) but in log-linear representation to zoom in on the high frequencies (the area inside the bold rectangle in (a)); (c) and (d) are as (a) and (b) but for the vertical wind components. Spectra of the measured wind components are represented using black lines whereas those of the corrected wind components are plotted with grey lines.

are generally used to compute fluxes by the EC method. Therefore, before correcting the wind velocity components for the EC method, the 50 Hz raw signals were first ‘re-sampled’ at 10 Hz using a five-point block average.

In order to test the procedure correcting for the ship’s motion, the turbulent spectra of the longitudinal and vertical velocity components multiplied by frequency in accordance with a $5/3$ power law, $f^{5/3} S_{uu}(f)$ and $f^{5/3} S_{ww}(f)$, respectively, are plotted in Fig. 6, before and after correction. This kind of representation tends to flatten the spectra from frequencies higher than 0.1 Hz, since the single spectrum is supposed to have a $-5/3$ power law at high frequencies (e.g. Kaimal *et al.* 1972), which means that these signals do follow the Kolmogorov theory in the inertial subrange. Thus, the spectra for the raw signals obviously indicate that the ship’s movements respond to the ocean swell. The spectra of the observed velocity components show a definite spectral peak at about 0.15 Hz induced by the ocean waves. The vertical velocity component seems to be more affected, with a broad and high peak extending from 0.08 to 0.25 Hz. On the other hand, no distinct peak remains in the spectrum of the corrected vertical velocity. As expected, after corrections both weighted spectra seem to be relatively flat between 0.1 and 1 Hz. However, some noise can be observed in both the raw and corrected wind components at frequencies higher than 1 Hz. It cannot be attributed to the corrections for the motion of the ship which intervene at lower frequencies.

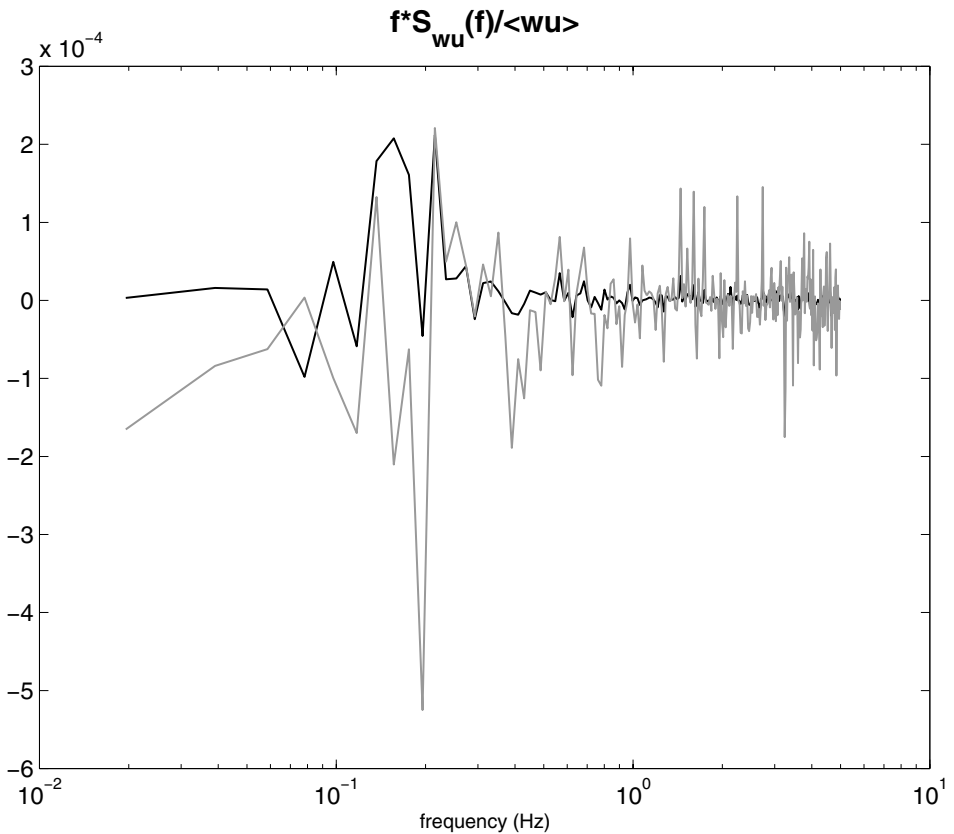


Figure 7. Example of a spectrum of the covariance of longitudinal and vertical wind components. The black line is for the covariance of uncorrected signals whereas the grey line is for the corrected cospectrum. See text for details.

The co-spectra have large fluctuations at low frequencies which is typical for all turbulence realizations, but they are again of ‘classical’ shape with no evidence of contamination from the ship’s motion. As a supporting example, the co-spectra of horizontal and vertical velocity components before and after correction are also shown in Fig. 7. Although the former co-spectrum indicates a large upward transport near the wave-induced frequency, the momentum is as expected transported downwards at low frequencies after corrections are applied; in Fig. 7, the uncorrected component is clearly contaminated by a spike at about the same frequency as the spectra (i.e. about 0.15 Hz). This spike dominates the signal and results in positive values of the longitudinal momentum fluxes when we integrate under the curve. Then, when we remove the ship’s motion from contamination of these turbulent signals, we obtain a co-spectrum with the correct sign. Earlier studies (Fujitani 1981; Katsaros *et al.* 1993) concerning corrections for the motion of ships, provide similar results on the spectra of corrected and uncorrected wind velocity components.

Another argument supports the efficiency of our corrections: the same correction procedure was applied during the POMME experiment on board the RV *L’Atalante* to realize flux measurements with conditional sampling (Brut *et al.* 2004). Latent-heat fluxes were measured on board the ship using a relaxed eddy accumulation system. This technique requires knowledge of the absolute vertical velocity in real time so as to select

the sampled air. Brut *et al.* (2004) compared their measurements with latent-heat fluxes computed using a standard bulk algorithm, and they observed a good agreement between the methods; this means that the air selection, and therefore the correction of the wind vertical velocity, is carried out well.

The time-averaged flux determined using the EC technique is regarded as the most direct estimate of the ensemble average flux, but this method is subject to sampling uncertainty (Wyngaard 1973). If j represents the parameter of interest (either u , q or potential temperature Θ), integrating the cospectrum $S_{wj}(f)$ over all contributing frequencies, f , gives the covariance and hence the turbulent flux. However, some variability in flux calculations can arise because the low-frequency contributions are not well sampled. In this case, applying a high-pass filter can minimize the scatter between fluxes. In our EC algorithm, this filtering removes the contribution of turbulent eddies whose length scale is greater than 5 km; the cut-off frequency, f_c , therefore, varies according to the relative wind speed U_r (where $U_r^2 = u_s^2 + v_s^2$) as $f_c = U_r/5000$. Throughout, turbulent fluxes are computed on 30-minute runs.

(ii) *Inertial dissipation technique.* The most attractive feature of the ID method is that it avoids the need for an explicit measurement of vertical velocity (Edson *et al.* 1991). These authors, as well as Oost *et al.* (1994) showed that this method is best adapted to regions of severe flow distortion, and in regions of weak distortion if the corrections needed for its effects are poorly known. In addition, it is possible to include airflow-distortion corrections using this method (Yelland *et al.* 1998; 2002; Dupuis *et al.* 2003) whereas corrections applied to the EC technique have not yet been investigated, due to the difficulty in simulating and evaluating the effects of distortion on turbulence levels.

The ID method uses the Monin–Obukhov similarity theory. It combines high-frequency measurements of meteorological signals and the use of the turbulent kinetic energy (TKE) and variance budgets to estimate the turbulent fluxes. Since the signals are analysed in the inertial sub-range, a frequency range which is minimally disturbed by ship movements, this technique is well suited for use on a RV. The problem of evaluating the turbulent fluxes lies in the determination of the friction velocity u_* , the dissipation rate of turbulent energy ε , and the destruction rates of half variances of temperature and humidity, N_θ and N_q , respectively. The ID algorithm we used is similar to that of Dupuis *et al.* (2003) which is itself adapted from that of Dupuis *et al.* (1997). The dissipation rates are calculated every 30 minutes from the density spectra of Θ , q and U_s , the latter being orientated along the mean relative wind, according to:

$$\varepsilon = (S_y/\alpha)^{3/2}(2\pi/U_r), \quad (5)$$

$$N_j = (S_j/\beta)\varepsilon^{1/3}(2\pi/U_r)^{2/3}, \quad (6)$$

where subscript j stands for Θ or q , S_y is the mean spectral energy at frequency f for the y parameter, multiplied by $f^{5/3}$ and α and β are the Kolmogorov and Corrsin constants, respectively ($\alpha = 0.55$, $\beta = 0.8$). The dissipation rates are calculated using the raw 50 Hz signals, from a frequency range which best matches the $-5/3$ power law within the inertial subrange. This frequency range is adapted to each 30-minute sample depending on an automatic test on the power law of the best fit to the spectrum. Turbulent fluxes are then derived using the equations of TKE and scalar variance budgets, normalized with the Monin–Obukhov similarity scales. The equation system

reads as (see for example, Dupuis *et al.* 1997):

$$u_* = [kz\varepsilon/\{\Phi_m(z/L) - z/L - \Phi_{imb}(z/L)\}]^{1/3}, \quad (7)$$

$$\overline{w'\Theta'} = \{kzu_*N_\Theta/\Phi_\Theta(z/L)\}^{1/2}, \quad (8)$$

$$\overline{w'q'} = \{kzu_*N_q/\Phi_q(z/L)\}^{1/2}, \quad (9)$$

$$L = -\Theta_v u_*^3 / (gk\overline{w'\Theta'_v}), \quad (10)$$

where Φ_m , Φ_Θ , Φ_q are the universal functions which represent the dimensionless vertical gradients of horizontal wind, temperature and humidity, respectively; z is the height of measurement above the sea, k is the Von Karman constant ($k = 0.4$), L is the Monin-Obukhov length, Θ_v is the virtual potential temperature, and g is the gravitational acceleration. The algorithm uses the formulation for Φ_m , Φ_Θ and Φ_q that was first proposed by Dyer (1974). In Dupuis *et al.* (1997) it was possible to use two options to solve the system: L could be determined using a ‘pure’ ID algorithm, with an iteration from neutral conditions ($z/L = 0$) continuing until a convergence threshold is reached on u_* , or L could be computed using a standard bulk formula. The first option appears to be quite restrictive since it implies a monotonically decreasing function $\Phi_\varepsilon = kz\varepsilon/u_*^3$ and the algorithm fails to converge in many cases. In the new algorithm (Dupuis *et al.* 2003), L is calculated using bulk formulae (with Large and Pond (1981) parametrizations) which does not significantly change the computed fluxes but significantly increases the number of the results.

In Eq. (7), $\Phi_{imb}(z/L)$ is an ‘imbalance’ term which accounts for the pressure and turbulent transport terms. This term, which represents the imbalance between local production and dissipation of TKE, was often neglected in previous studies (Large and Pond 1981; Edson and Fairall 1994). According to Yelland and Taylor (1996) this term was apparently a function of both z/L and the wind speed. Dupuis *et al.* (1997) also observed that the use of this imbalance term was necessary to minimize the dependence of the C_{Dn} values on stability for near-neutral to unstable conditions. Recently, Edson and Fairall (1998), who investigated updated forms of the dimensionless universal functions of the TKE budget, included a significant imbalance term. Their study found that for slightly unstable conditions production exceeds dissipation by as much as 17%. A possible explanation for this might be that over developing waves part of the energy flux generates waves and currents, rather than being dissipated into thermal energy. On the other hand, Smedman *et al.* (1999) clearly indicate that at low wind speeds swell effects may cause a large imbalance in the TKE budget. Papers by Grachev and Fairall (2001) and Drennan *et al.* (1999) confirm this latter result. Actually, the recent published formulas for the imbalance term in near-neutral conditions show good agreement (see Taylor and Yelland 2000), lying between the Dupuis *et al.* (1997) and Edson and Fairall (1998) parametrizations. Taking a contrary view, Taylor and Yelland (2000) argue that the use of an imbalance term cannot remove the apparent stability dependence. However, they chose a Kolmogorov constant which is supposed to account for, or minimize, this imbalance term. In the case of EQUALANT99 we opted for the value suggested by Dupuis *et al.* (2003), where $\Phi_{imb}(z/L) = -0.5z/L$. Since this formula tends towards zero at near-neutral stratifications, we do not expect that the imbalance term will significantly change the relationship of the mean neutral drag coefficient versus the mean wind speed, since very few extreme stratifications were encountered during EQUALANT99.

(iii) *Retrieval of bulk coefficients from fluxes.* Since the bulk coefficients clearly depend on the measurement height and the atmospheric stratification, it is customary

to choose 10 m as the conventional height and a neutral atmosphere as standard conditions. So, C_{Dn} , C_{Hn} and C_{En} are the 10 m neutral exchange coefficients for the wind, temperature and moisture, respectively. They are derived from turbulent fluxes and the neutral mean meteorological parameters at 10 m: U_{10n} , Θ_{10n} and q_{10n} ; the subscript 10n stands for neutral atmospheric conditions at a height of 10 m. The neutral mean meteorological parameters are calculated from the measured ones using the relations between the gradients of wind, temperature and humidity and empirical stratification functions (Φ_j). Then, integrating these functions leads to U_{10n} , Θ_{10n} and q_{10n} (Dupuis *et al.* 1997). The neutral exchange coefficients are obtained as follows:

$$C_{Dn} = \frac{\overline{w'u'}}{U_{10n}^2}, \quad (11)$$

$$C_{Hn} = \frac{\overline{w'\Theta'}}{U_{10n}(\Theta_S - \Theta_{10n})}, \quad (12)$$

$$C_{En} = \frac{\overline{w'q'}}{U_{10n}(q_S - q_{10n})}, \quad (13)$$

where subscript S stands for the sea surface. The ocean surface current is generally neglected in bulk formulae except when significant currents are observed. Then, the parametric relations can be established between the neutral exchange coefficients and the absolute wind speed U_{10n} .

3. CORRECTIONS FOR AIRFLOW DISTORTION

(a) *Physical simulations in the water tank*

(i) *Introduction.* The results presented in this section are from physical simulations of airflow distortion around a model of RV *La Thalassa* in a water channel. The analysis of the EQUALANT99 dataset pointed out a bias in the wind speed magnitude and in the vertical wind velocity component measured at the top of the foredeck mast. This latter error induces a lift of the airflow which results in a non-zero angle of the airflow direction at the sensor location, in the vertical plane. Hereafter, this angle is called the incidence angle. Since these disruptions lie behind large errors in flux computation, this study is aimed at quantifying the airflow distortion. Simulations in a water channel represent a further analysis of airflow distortion studies that started at CNRM with numerical simulations for the FETCH experiment (Nacass 1999; Dupuis *et al.* 2003) run with the Fluent 5 code (Fluent Inc.).

Although the FETCH and EQUALANT99 campaigns involved two different RVs (*L'Atalante* and *La Thalassa*, respectively), both ships are very similar, and their shape and instrumentation were reproduced similarly in these experiments (see Weill *et al.* 2003). In both cases, the same sonic anemometer was located at the top of the same mast, about 18 m above sea level (hereafter a.s.l.) on the front deck. In addition, the positions of sensors and electronic boxes were almost identical during these two campaigns. The advantage of physical simulations compared to numerical ones lies in their capacity to reproduce the detailed structure of the mast (Fig. 4). For this study, the shape of the mast with the sensors and electronic boxes was carefully reproduced, and this allows us to evaluate the impact of the mast on airflow distortion. Butet (2001) concluded that the airflow distortion strongly depends on the blocking effect caused by the mast structure and the experimental configuration of the ship. Physical simulations enable

us to optimize the location of instruments and sensors on the mast in order to minimize airflow distortion. For instance, for the POMME campaign (Memery *et al.* 2005), results from Butet (2001) show that the configuration of the mast instruments was improved where possible: devices that caused most disturbance to the airflow were miniaturized or moved.

(ii) *Upstream flow calibration.* Physical simulations in a water channel rely on the similarity theory: the atmospheric boundary layer is reproduced by a water flow. When the reduction scale, E , is chosen, it represents a direct connection between the true atmospheric values (subscript a) and those simulated in the water flow (subscript w). The similarity length scale is defined as:

$$z_a/z_w = z_{0a}/z_{0w} = 1/E, \quad (14)$$

where z represents height and z_0 is the roughness length.

The water channel of CNRM consists of a free surface corridor of length 30 m, width 3 m and depth 1.6 m. In order to take into account the water channel size, the airflow around the ship is simulated by a water flow around a 1/60 scale model of the RV (Butet 2001). This corresponds to the following dimensions for the ship model: length 1.22 m, width 0.25 m and height 0.26 m. Special devices allow us to establish vertical gradients of wind velocity and density. In this case, a neutral stratification is simulated. The upstream wind profile (i.e. the undisturbed profile) is developed by friction of the flow over a calibrated roughness at the onset of the corridor. The flow velocity outside the boundary layer can be adjusted accurately up to 0.60 m s^{-1} in the water tank with a turbulence weaker than 1%. Since the experimental chamber is glazed on each side, we can see the flows by illuminating micro-particles sown within them by laser light. The movement of particles is then recorded by video camera so as to retrieve their trajectory from successive images. Figure 7 shows an example of a picture using laser light of the modelled RV with a full solid mast: an uplift in the ‘air’ flow is clearly observed at the top of the mast. This technique was then reproduced with the detailed mast so as to measure the difference, Δh , between the measurement level (at the top of the mast) and the original (undisturbed) level of air parcels.

Generally, Δh is considered to be as important as the bias in the measured wind speed, and it has to be accounted for when computing fluxes. Actually, to apply corrections for this vertical displacement, z has to be replaced by $z - \Delta h$ in Eqs. (7) to (10). Furthermore, Yelland *et al.* (2002) showed that the vertical uplift height Δh varies with azimuth angle. In their paper, they reported that Δh can increase from about 1 m when the ship is facing the mean wind to about 2 m for an azimuth angle of 30° , depending on the ship structure and on the location of the sonic anemometer. Unfortunately, in our study the impact of azimuth angle on Δh was not tested: the constant value $\Delta h = 0.90 \text{ m}$, which was determined for a 0° azimuth angle, was also used to correct fluxes whatever the azimuth and incidence angles. Only flux samples for which the wind direction varies between $\pm 30^\circ$ with respect to the ship’s axis are selected to determine new parametrizations, so the variation of Δh related to the wind azimuth may have lesser impact since this variation is found to increase with high azimuth angles. This is discussed in subsection 3(b).

In the water channel, it is possible to simulate a standard marine boundary layer corresponding to neutral stratification in a real case. The upstream flow, which is considered as a reference for the wind speed, is obtained by natural development of the boundary layer over a smooth floor at the onset of the water channel. This ‘undisturbed’ flow is defined at about 1 m upstream of the model, which corresponds to 60 m in

real conditions. For these simulations the water flows in the channel at a speed of 0.39 m s^{-1} which corresponds to a real upstream wind of 15 m s^{-1} . Within the boundary layer we reproduced a fully turbulent flow for which the Reynolds number associated with the ship length is 10^5 . The features of this simulated boundary layer when converted to real conditions are as follows: a surface layer height, δ , of 10 m; a friction velocity, u_* , of 0.60 m s^{-1} ; and a roughness length, z_0 , of $1.8 \times 10^{-3} \text{ m}$. The desired wind speed profile is obtained using a coefficient of 0.15.

Another important parameter is the blockage ratio; this is defined as the ratio of the frontal area of the body to the tunnel cross-sectional area. It characterizes the flow acceleration artificially induced by the constriction of the tunnel walls. In this study, the blockage ratio has been calculated for azimuth angles of 0° and 30° , and in both cases it is weaker than 0.009. According to Castro and Robins (1977), this should lead to a maximum acceleration of 0.9% on the simulated flow speed in the water channel. This error remains negligible compared to the estimations of airflow distortion.

(iii) *Measurement methodology.* The three components of the flow speed and the various velocity profiles are measured using a laser Doppler anemometer mounted on a mobile bench along the channel. Laser anemometry is a non-intrusive technique, which provides velocity measurements with an accuracy of up to 98%. The flow speed is measured each time a particle comes through the ‘measurement volume’. This volume size is $0.3 \times 0.05 \times 0.05 \text{ cm}^3$ which corresponds to $18 \times 3 \times 3 \text{ cm}^3$ in true dimensions, so it can be approximately compared to that of the sonic anemometer. Data are recorded at a sampling rate of 50 Hz during 112 s in the simulations, they are then averaged over volume and time to obtain a reliable velocity estimate. Inside the channel, the velocity measurements were performed along a vertical profile whose origin is chosen at the sonic anemometer level. Although the sonic anemometer is located about 80 cm in front of the mast, it is in the disturbed flow; actually, the effect of flow compression by the mast boxes and structure can even be observed upstream.

In order to quantify airflow distortion around the RV *La Thalassa*, the longitudinal flow component in the mean flow direction, U_m , and the vertical wind component, w_m , were first measured and then, since these data are synchronized, the incidence angle, I_m , could be determined, with an accuracy of 4% using the following law:

$$I_m = \tan^{-1}(w_m/U_m) \quad (15)$$

where a positive I_m means an uplift of the airflow with respect to the sensor. In fact, three terms are involved in the instantaneous I_m , which can be expressed as:

$$I_m = \tan^{-1}(w_\infty/U_{s\infty}) + \theta + \delta I, \quad (16)$$

where the first term on the right-hand side corresponds to the angle I_∞ between the mean flow and the horizontal at ‘infinity’ (i.e. undisturbed) upstream, and δI is the distortion angle due to the ship and the instruments. Since the upstream flow in the water channel is horizontal ($w_\infty = 0$), the various angles of incidence of the upstream flow are simulated by varying the pitch angle of the model.

Several experimental conditions were used to characterize the distortion in the water channel: three inlet azimuth angles ϕ (0° , 15° and 30°) and five pitch angles (-10° , -5° , 0° , 5° and 10°). It is hypothesized that the effects are symmetrical on the left and right sides of the ship. The simulations reveal that both the ship’s body and the mast with the sensors and boxes attached distort the flow. These effects were determined from twin simulations, with and without the mast on the model. The aerodynamic envelope of the ship decreases the wind speed by up to 2.5% above the deck for bow-on flow

TABLE 2. CORRECTION COEFFICIENTS DEDUCED FROM PHYSICAL SIMULATIONS IN A WATER CHANNEL FOR VARYING AZIMUTH ANGLES

Wind azimuth angle (degrees)	Distortion angle δI (degrees)	Correction coefficients for mean wind speed (m s^{-1})
0	6.4	1.103
15	6.6	1.087
30	5.9	1.031

TABLE 3. CORRECTION COEFFICIENTS DEDUCED FROM PHYSICAL SIMULATIONS IN A WATER CHANNEL FOR VARYING INCIDENCE ANGLES

Incidence angle I_m (degrees)	'Airflow angle' $(I_\infty + \theta)$ (degrees)	Distortion angle δI (degrees)	Correction coefficients for mean wind speed (m s^{-1})
16.7	10	6.7	1.014
11.6	5	6.6	1.054
6.4	0	6.4	1.103
0.5	-5	5.5	1.119
-5.0	-10	5.0	1.128

See text for definitions.

assuming a zero pitch angle, and then the mast amplifies this perturbation by up to 10% at the sonic location for the same conditions. Tables 2 and 3 also show that the distortion is very sensitive to both the wind incidence and azimuth angles. The effect of the flow incidence angle can reach 12% of the wind velocity when the ship's bow leans forward (Table 3) because in this case the ship's bow presents a large surface area to the airflow. On the other hand, when pitch is positive the ship's bow is lifted backwards and the blocking effect is less important. The impact of distortion also varies with azimuth angle (Table 2): the wind speed decreases when ϕ increases (Butet 2001; Brut *et al.* 2002). There is a blocking effect of the airflow due to the ship's superstructure when the RV faces the wind.

(iv) *Comparison with in situ data.* Before applying corrections to the wind speed values to account for airflow distortion, the results obtained in the laboratory were tested using the EQUALANT99 dataset. A simple way to compare the results of physical simulations in the water channel and *in situ* measurements was to compute the mean measured incidence angle for each 30-minute sample, using Eq. (15), and to study its dependency on the azimuth angle. Assuming a horizontal flow ($w_\infty = 0$) for measured samples, the mean incidence angle is easily determined. Then, considering similar conditions for both *in situ* measurements and simulations, it becomes relevant to compare the measured and simulated parameters. In Fig. 8 the measured incidence angle, as well as averages and standard deviations, is plotted against azimuth angle over bins of 10° . The simulated incidence angles are also presented for the three inlet azimuth angles (0° , 15° and 30°). A general good agreement is observed between simulations and *in situ* data, though experimental simulations in the water channel tend to underestimate the incidence angle for azimuth angles greater than 20° . However, it is more difficult to study the incidence angle dependency on the mean pitch, because pitch averaged over 30 minutes is no longer representative of the ship motion. The results provided by this comparison show that the mean incidence angle is well reproduced in the water channel for similar conditions to those observed during the campaign, and this validates the physical simulations in the water channel.

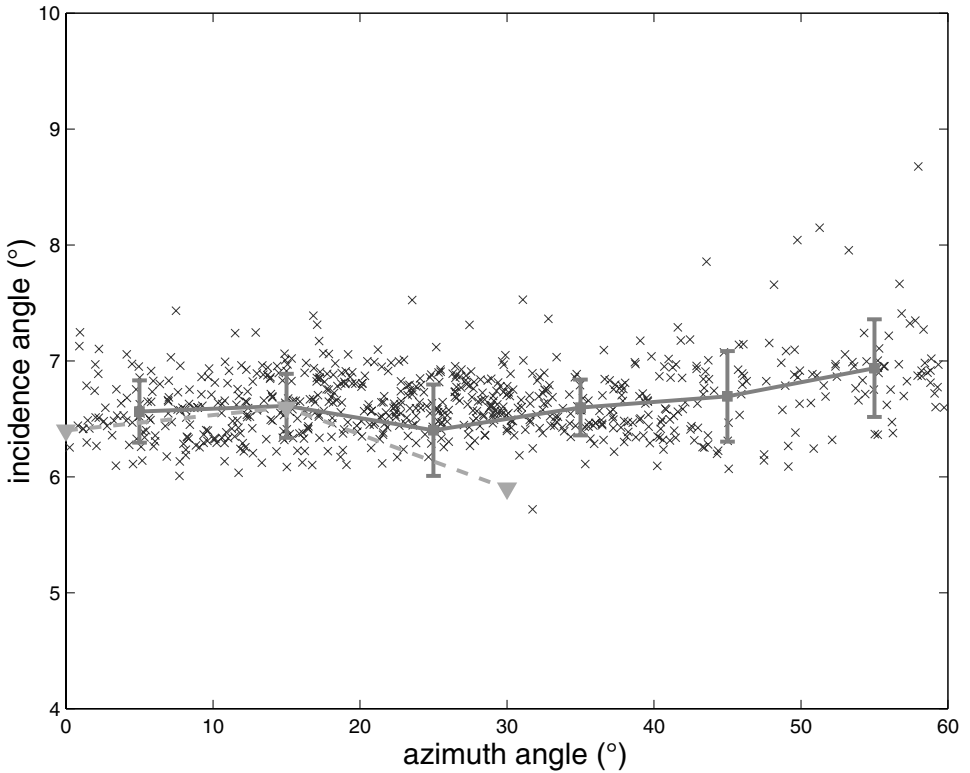


Figure 8. Incidence angles measured during the EQUALANT99 experiment from 14 July to 22 August 1999, averaged over 30-minute samples plotted against azimuth angles (crosses). The solid line corresponds to mean values over bins of 10° . The dashed grey line represents the simulated incidence angles, obtained in a water channel. Vertical lines correspond to standard deviations.

(b) Method for wind corrections

The physical simulations provide discrete correction coefficients (Tables 2 and 3) for relative wind speed, according to the incidence and azimuth angles. In order to quantify the correction, a polynomial surface $\alpha(I_m, \phi)$ was deduced from the experimental coefficients and applied to the measured relative wind velocity, U_r . For azimuth angles varying between $\pm 30^\circ$ and angles of incidence varying between -4° and $+18^\circ$, it is expressed as:

$$\alpha(I_m, \phi) = -8.127 \times 10^{-5} \phi^2 - 2.53 \times 10^{-4} I_m^2 - 2.38 \times 10^{-3} I_m + 1.113 \quad (17)$$

$$U_{\text{corrected}} = \alpha(I_m, \phi) \times U_r. \quad (18)$$

When angles are observed outside this range, the airflow distortion is neither known nor quantified. In addition, samples for which the mean absolute angle of wind azimuth is greater than 30° are rejected in the further analysis.

Pitch variability, which is mainly related to swell, has a dominant period of 5 to 10 s. The relative wind speed signal is corrected for airflow distortion at 1 Hz in order to properly take into consideration the effects of pitch. We consider that it is the fastest frequency possible at which to carry out corrections, since the physical simulations in the water channel cannot reproduce fluctuations representing small eddies (i.e. the turbulent frequencies; Butet (2001)). Thus the correction coefficients established from the physical simulations are not valid for high-frequency wind fluctuations. This means

that the simulated distortion corrections cannot be used when fluxes are computed by EC. Indeed, this technique should include corrections calculated at the same frequency rate as the covariance computation (10 Hz). In addition, correcting EC fluxes for flow distortion tackles another problem which concerns the most energetic eddies. These eddies, which contribute greatly to the flux using the EC method, are of the same order of length as the height of the platform, so they may be distorted by the structure itself. This increases the difficulty of estimating the impact of airflow distortion on the EC fluxes.

In the ID algorithm some changes were required to account for the airflow distortion corrections. The method proposed by Yelland *et al.* (1998) was followed:

- The measurement height (about 18 m a.s.l.) is corrected for the vertical displacement of airflow, Δh . This displacement is supposed constant for azimuth angles smaller than 40° off the bow and amounts to 0.9 m. The impact of using a constant Δh is discussed in subsection (c).

- The determination of neutral bulk coefficients requires values of U_{10n} , the mean wind speed at 10 m height for neutral atmospheric conditions. To account for airflow disturbance, U_{10n} is computed as follows: the corrected relative wind speed is obtained using Eqs. (17) and (18) at 1 Hz, and the mean relative wind speed is computed over a 30-minute period; the wind speed in the earth frame is calculated from this corrected wind speed, and then corrected to represent neutral conditions at 10 m height. The U_{10n} calculation is performed using the method of Dupuis *et al.* (2003).

- The computation of the dissipation rates, which requires the mean relative wind speed, U_r , in order to convert wave number into frequency, is carried out using the uncorrected values of U_r , since turbulence is assumed to be unaffected by airstream distortion in the inertial sub-range. This assumption was studied by Yelland *et al.* (1998, 2002), who determined the required time for the mean airflow to be lifted by Δh from its upstream level and compared it to the correlation or ‘memory’ time of turbulence. This latter appeared to be greater than the displacement time, which means that the turbulence has not adjusted to the vertical displacement by the time the flow reaches the anemometer site. This is confirmed by Yelland *et al.* (2002) for bow-on flows, but it does not appear to be the case for beam-on flows.

(c) Results and verification of the flow distortion corrections

(i) *Validation of physical simulations.* In Fig. 9 the effects of the corrections for airflow distortion on the mean wind speed for the EQUALANT99 dataset are shown. Corrected mean wind velocities, computed over a 30-minute period, are expressed as a function of measured U_r . The corrected mean wind is about 6% greater than the measured one; this mean increase is represented by the dashed line in Fig. 9. We can see that this correction induces an angle of incidence of 7 to 8° , and a correction varying between 5 and 10% (see Table 3).

In order to evaluate the impact of corrections derived from water channel simulations, we intended to compare them with the results on airflow distortion obtained by numerical simulations performed on the RV *L’Atalante* for the FETCH experiment. This comparison seems to be valid because the RVs in both campaigns are of very similar shape and their instruments were placed at the same locations on the masts. RV *L’Atalante* is 85 m long from stem to stern and 16 m wide, whereas RV *La Thalassa* is 73 m long and 15 m wide; in both cases, the top of the mast is 18 m a.s.l. A possible means to test the corrections for airflow distortion derived from the two kinds of simulations is to apply the correction function proposed by Dupuis *et al.* (2003; their Eq. (1))

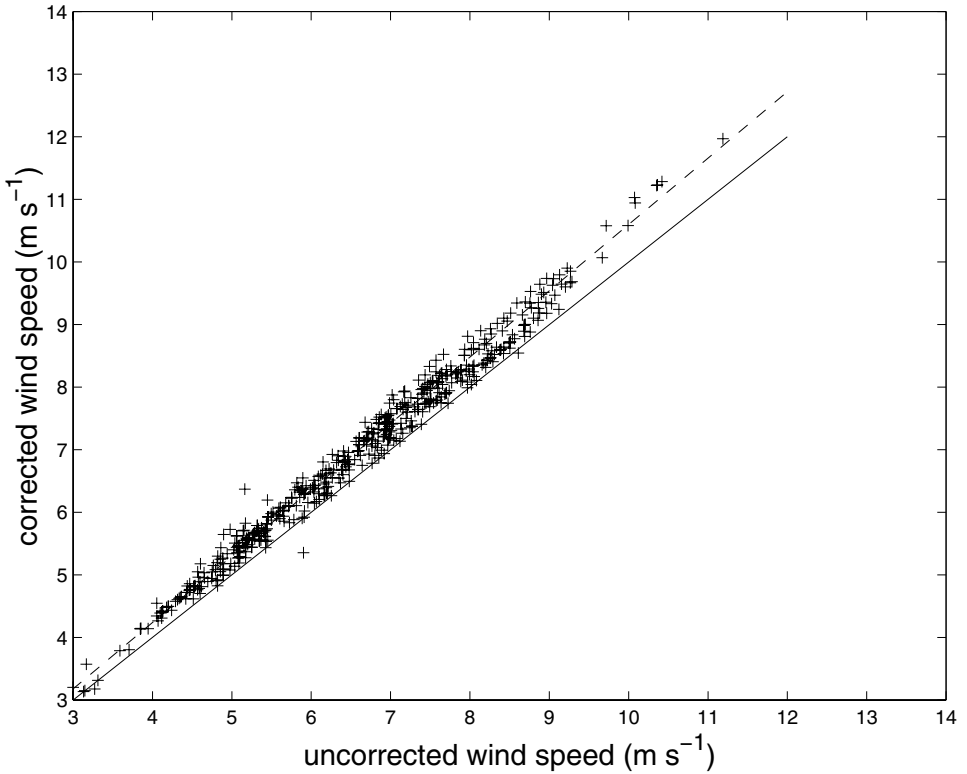


Figure 9. Effect of the correction for airflow distortion on the mean wind speed during the EQUALANT99 experiment from 14 July to 22 August 1999. Corrected wind speeds are plotted versus uncorrected values. The solid line is a one-to-one slope and the dashed line corresponds to an increase of 6%.

which depends on the azimuth angle, to the raw dataset of EQUALANT99. The mean wind speed values corrected using the FETCH equation are denoted by U_{CFE} whereas those corrected using the EQUALANT99 method are U_{CEQ} . Their relative difference is presented in Table 4; it can be seen that it remains small whatever the azimuth angle. It varies between -0.5% for small azimuth angles of $0^\circ-10^\circ$ to 1.25% for azimuth angles of $25^\circ-30^\circ$. The EQUALANT99 correction provides greater mean wind velocities than the FETCH correction when the ship faces the wind ($0^\circ-10^\circ$). The bias between both methods is very small, and this result is very satisfactory since we expect a similar impact of airflow distortion during both campaigns: airflow distortion is indeed induced by the ship structure and the shape of the mast, and the effects were almost the same in the two campaigns.

(ii) *Discussion of the vertical displacement Δh .* Yelland *et al.* (2002) showed the importance of the vertical displacement of the flow due to distortion. Using numerical simulations, they measured this displacement for various azimuth angles and observed that the vertical displacement of the flow at the sonic anemometer, located on the foremast platform, varied from 1.2 to 1.7 m for RV *Darwin* and from 1.1 to 1.8 m for RV *Discovery* as the direction of the flow changed from bow-on to 30° off the bow. Since the vertical displacement was determined only for bow-on flow in our case, we intended to evaluate the impact of a constant Δh on the airflow distortion corrections. In Fig. 10, the mean C_{Dn} values are plotted against U_{10n} for several groups

TABLE 4. COMPARISON OF AIRFLOW DISTORTION CORRECTIONS APPLIED TO THE EQUALANT99 DATASET

Azimuth angle ($^{\circ}$)	Bias ($U_{CFE} - U_{CEQ}$)/ U_{CEQ} (%)
0–5	–0.57
5–10	–0.17
10–15	0.31
15–20	0.81
20–25	1.11
25–30	1.24
30–35	1.16
35–40	–0.02

Comparisons are between using the FETCH corrections (see Eq. (1) in Dupuis *et al.* (2003)) and the EQUALANT99 corrections (see Eqs. (15) and (16) in this paper). The bias between wind speed corrected with the FETCH method (U_{CFE}) and that corrected with the EQUALANT99 method (U_{CEQ}) is very small (less than 1%). See text for further details.

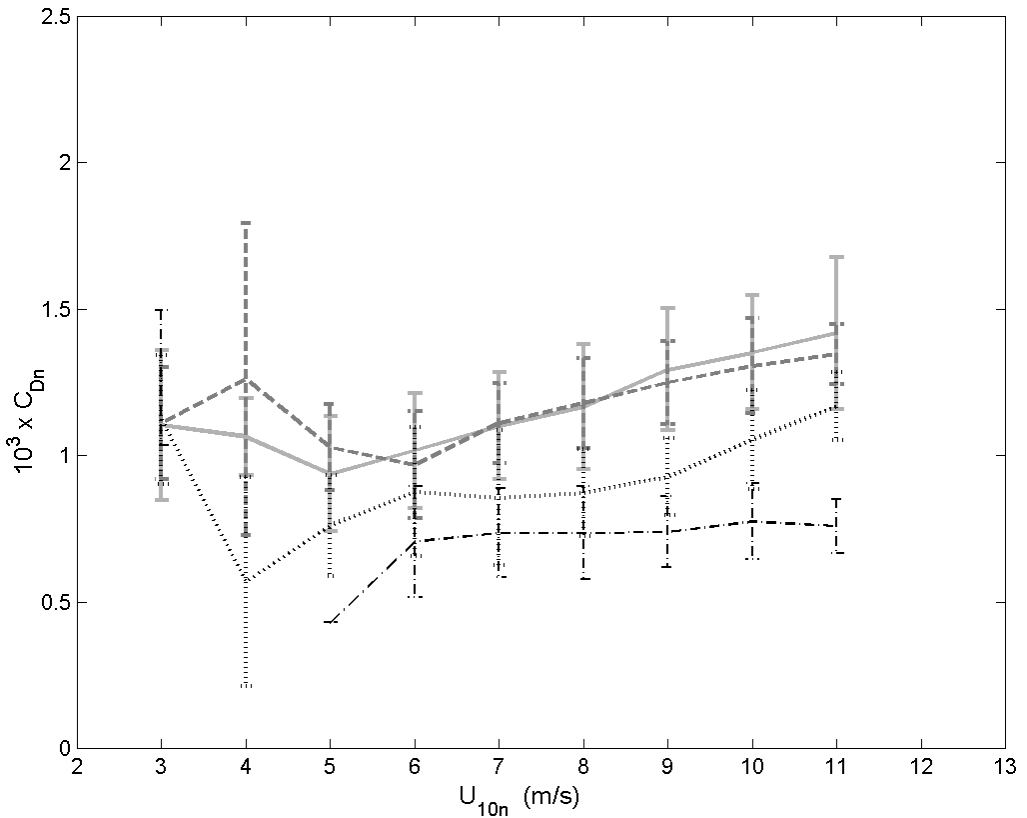


Figure 10. Mean neutral drag coefficients (C_{Dn}) as a function of the neutral wind speed (U_{10n}) for several ranges of azimuth angle. The solid line is for bow-on flows (0° – 20°); the dashed line is for azimuth angles varying from 20° to 40° off the bow; the dotted line corresponds to the range 40° – 60° off the bow; and the dash-dotted line is for the range of azimuth angles greater than 60° off the bow. Samples for which the mean wind azimuth angle is smaller than 40° are corrected for airflow distortion. Vertical lines correspond to standard deviations.

of azimuth angles. For bow-on flows and flows at 20–40° off the bow (i.e. flows that have been corrected for distortion), the mean C_{Dn} curves are very similar, whereas for greater azimuth angles for which no correction is applied the C_{Dn} parametrization is below the two former curves. The difference between these curves induces a loss in the momentum-flux computation when the flow direction is greater than 40° off the ship's bow. The difference between groups of mean C_{Dn} can be attributed to two effects: first, the constant vertical displacement in the airflow distortion corrections; and second, the mean wind speed bias related to the fact that only one part of the dataset is corrected for airflow distortion. Dupuis *et al.* (2003), who corrected their data for a larger range of wind azimuth angles, used the same method to evaluate the likely variation of Δh with azimuth angle. However, in our case, a severe criterion was applied to the dataset before the new parametrization of the drag coefficient was established, and samples corresponding to azimuth angles greater than 40° were rejected. Therefore, since the estimated vertical displacement is only likely to vary for the greater azimuth angles which correspond to rejected samples, the use of a constant vertical displacement in the airflow distortion corrections was considered to be sufficient in the determination of new parametrizations that account for airflow distortion.

(iii) *Impact on the transfer coefficients.* The impact of corrections is clearly observed on the bulk coefficients. Figure 11(a) represents the uncorrected versus corrected neutral drag coefficients C_{Dn} (for identical U_{10n}), both derived from ID fluxes. On both axes, values have been averaged over 1 m s⁻¹ bins of U_{10n} . In Fig. 11(b), the same representation is used for the neutral bulk coefficients for evaporation C_{En} . Due to the low values of sensible-heat fluxes over the ocean and the resulting high-frequency noise on the sonic temperature signal, C_{Hn} coefficients computed using the ID technique are highly scattered and thus are not presented here. The standard deviation computed for each bin is represented by a horizontal error-bar for uncorrected values and a vertical bar for corrected values.

First of all, it must be noted that for both the C_{Dn} and C_{En} coefficients, the standard deviations are smaller after corrections for flow distortion. This clearly means that the correction reduces the scatter of neutral coefficients as a function of U_{10n} . This result is very encouraging concerning the consistency of these corrections, since it leads to more accurate parametrizations of bulk fluxes.

We observe in Fig. 11(a) that the drag coefficients increase with wind speed and that they are reduced by about 20% when applying the corrections for airflow distortion. At low wind speeds, C_{Dn} seems to be less affected by airflow disturbance, but many uncertainties remain concerning its behaviour during convective events. The C_{En} values (Fig. 11(b)) also increase with wind speed, unlike results presented by Large and Pond (1982) and DeCosmo *et al.* (1996) but in agreement with the results of Dupuis *et al.* (2003). This behaviour clearly appeared when a refractometer (Delahaye *et al.* 2001) was used to record humidity fluctuations aboard RVs during previous French air–sea experiments: FETCH (Hauser *et al.* 2003), EQUALANT99 (Gouriou *et al.* 2001), and POMME (Memery *et al.* 2005). Refractometers are more efficient than the more typical Lyman-alpha hygrometers on board RVs. Simulations and observations showed that salt deposit and spray had negligible effect on measurements made by the refractometer (Eymard *et al.* 1999; Delahaye *et al.* 2001). In addition, the dependence of the Dalton number on the wind speed is increased by the ‘1 Hz correction’ method applied on the EQUALANT99 dataset to account for airflow distortion, as explained below.

In order to evaluate the impact of this new method of correcting airflow distortion, we compared the 1 Hz corrections with the correction carried out in previous studies,

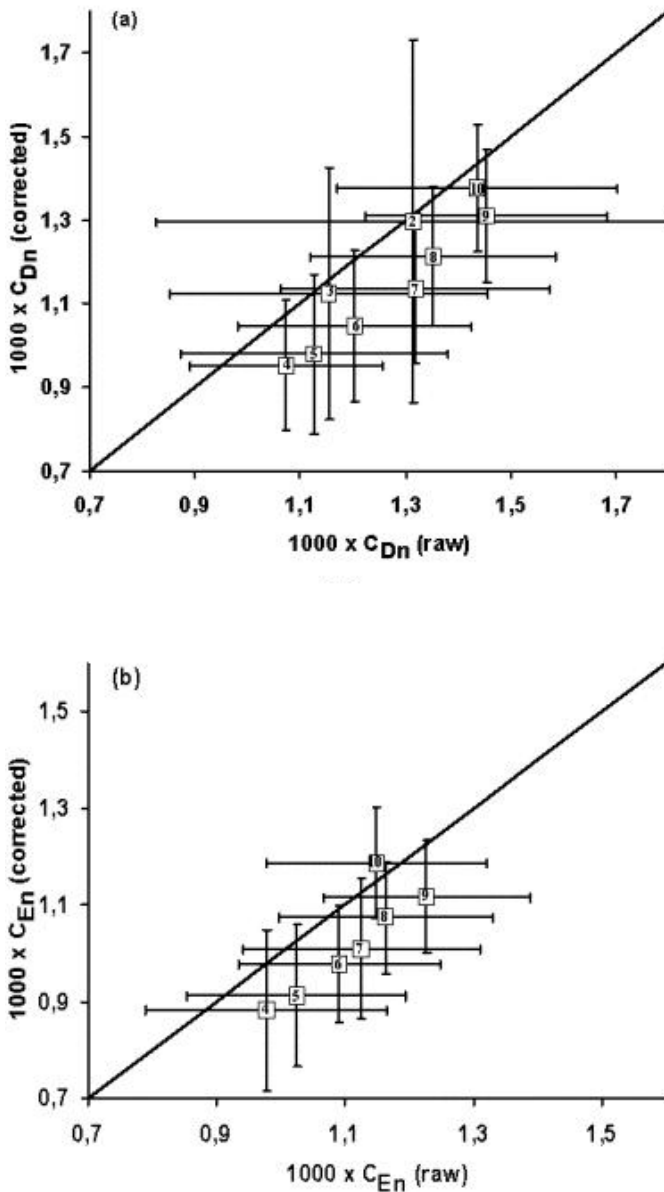


Figure 11. (a) Neutral drag coefficients (C_{Dn}) corrected for airflow distortion as a function of the uncorrected values for several ranges of wind speed. The scatter is represented by error-bars. These values are obtained from inertial dissipation fluxes, and they are averaged over bins of 1 m s^{-1} for the 10 m wind speed with neutral stability, U_{10n} . The corresponding wind speed bin is indicated on each square in m s^{-1} ; (b) as (a), but for the 10 m neutral exchange coefficient for moisture, C_{En} .

which consisted of applying a single correction to the mean wind speed per flux sample (Yelland *et al.* 1998; Dupuis *et al.* 2003). The results are presented in Fig. 12. It is evident that both corrections diminish the transfer coefficients relations to the wind speed compared to the uncorrected parametrization. It also appears that the scatter of the transfer coefficients is slightly larger for the mean correction samples; the 1 Hz correction seems to reduce the uncertainties in estimates of the transfer coefficients.

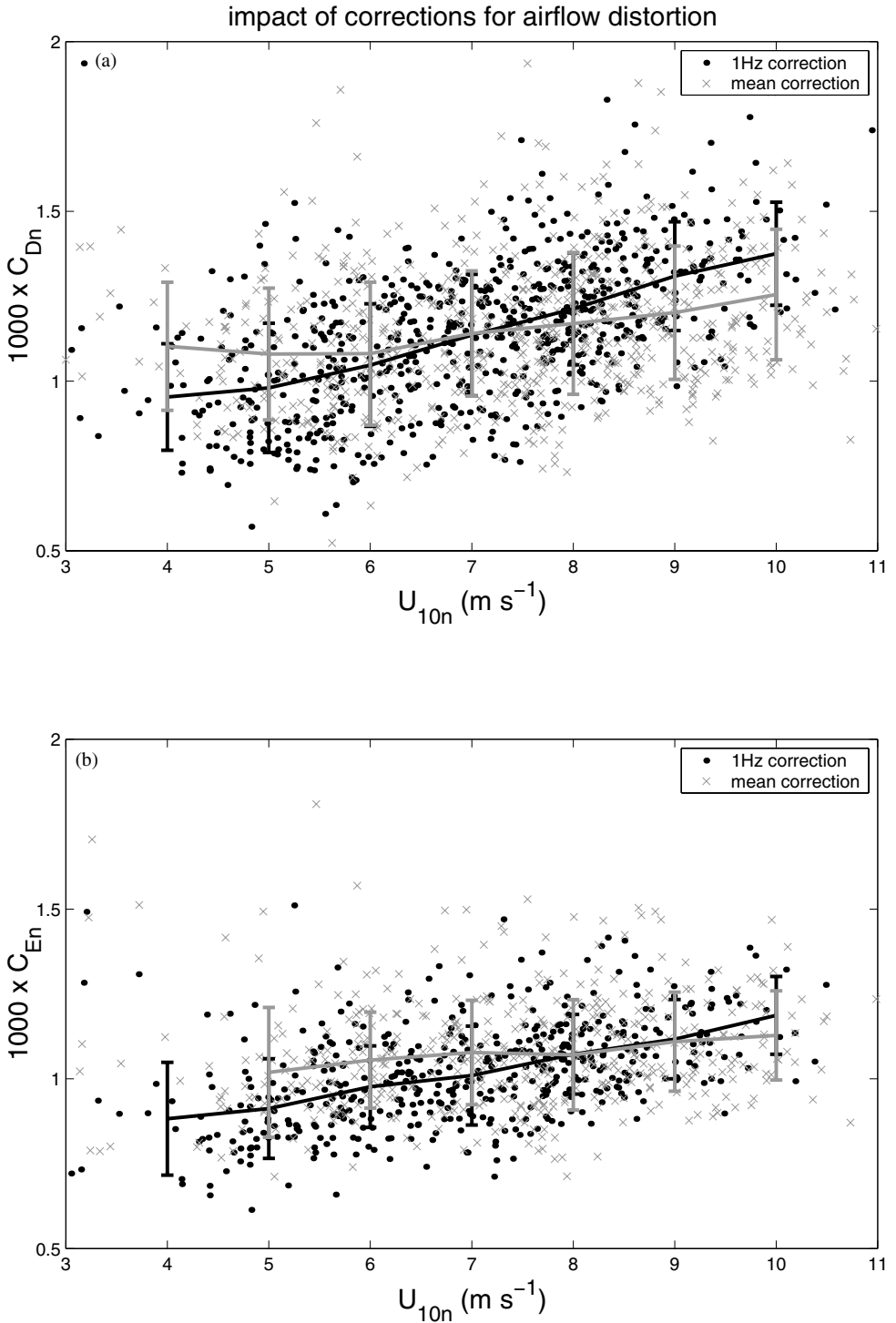


Figure 12. Comparison of the 1 Hz correction and mean wind correction as performed in previous studies: (a) neutral drag coefficient, C_{Dn} , versus the neutral wind speed at 10 m, U_{10n} ; (b) as (a) but for the exchange coefficient for moisture, C_{En} . Scatter is represented by error-bars. These values are obtained from inertial-dissipation fluxes and they are averaged over bins of 1 m s^{-1} for U_{10n} . Black dots are for 1 Hz corrections and grey crosses represent samples corrected with the mean wind corrections.

However, the 1 Hz correction emphasizes the dependence of the transfer coefficients on the neutral wind speed. This is particularly striking for the Dalton number, for which a constant value is generally used. This result is rather surprising, although it can be explained by the fact that the wind speed measured at the anemometer site is strongly dependent on the ship's angle with respect to the 'sea plan' (i.e. the pitch angle). Butet (2001) showed that whether the pitch angle is positive or negative the effect on the mean flow is the opposite: it is decelerated when the angle is negative and can even be accelerated when the pitch is positive. Therefore, it turns out that including the effect of the pitch on the flow distortion corrections leads to a difference between the single correction on the mean wind speed and the average of the 1 Hz corrections. This effect echoes on the neutral coefficients, mainly via the wind speed, and it increases the dependence of the transfer coefficients on the mean wind speed while reducing the scatter between samples.

4. TURBULENT FLUXES AND THEIR PARAMETRIZATION

(a) *Comparisons of flux measurement methods*

Differences are observed between flux calculations made using the EC and ID techniques (Wucknitz 1979; Large and Pond 1982; Edson *et al.* 1991). This is particularly true when fluxes are measured on board RVs. During EQUALANT99, fluxes computed by the two methods were compared to each other and to bulk estimates provided by the Fairall *et al.* (1996) algorithm (version 2.5). This computational package, developed for the equatorial Pacific Ocean, uses an iterative resolution of the bulk system and does not rely on polynomial relations between the exchange coefficients and the wind speed.

Scatter plots of turbulent fluxes are shown on Figs. 13 and 14, and the features of the inter-comparison of EC and ID calculations are summed up in Table 5. The first striking feature of this comparison concerns the EC momentum flux, u_*^2 , which is more than 30% lower than the ID and bulk fluxes. This result is all the more surprising in that ID and bulk fluxes have been corrected for airflow distortion, unlike the EC values. For the momentum fluxes the slope of the linear regression is far from 1:1 when EC measurements are compared to bulk ones (0.62) or when ID measurements are compared to EC ones (1.31) although in both cases, a high correlation coefficient is obtained ($r = 0.85$ and 0.84 respectively). On the other hand, ID and bulk momentum fluxes are of similar orders of magnitude with an excellent correlation between the two methods. Regarding the results of the momentum flux comparisons, the differences between EC measurements and other estimates are not constant (the intercept of linear regression is small) but the bias is related to the flux magnitude (high slope of the linear regression). At low wind speeds a high scatter is observed on Fig. 13.

One of the reasons invoked to explain such differences is imperfect correction of the horizontal wind components due to a lack of information regarding horizontal ship movement. Looking back at Fig. 6, one can see that the spectrum of corrected covariance (wu) remains noisy at the low frequencies (0.05–0.2 Hz) contributing to EC measurements. In addition, the surface between the x -axis and the co-spectra shape (which is proportional to the flux) is still small and noisy after corrections, although it has the correct sign. For instance, the co-spectra of $\langle w\theta \rangle$ and $\langle wq \rangle$ present a more typical shape and they are highly energetic at low frequencies. Since the loss of the flux appears at low frequencies, we attribute it to inadequate compensation for the ship's motion when corrections are applied to the horizontal wind components. Actually, the navigation parameters are recorded separately from, and at lower frequencies than,

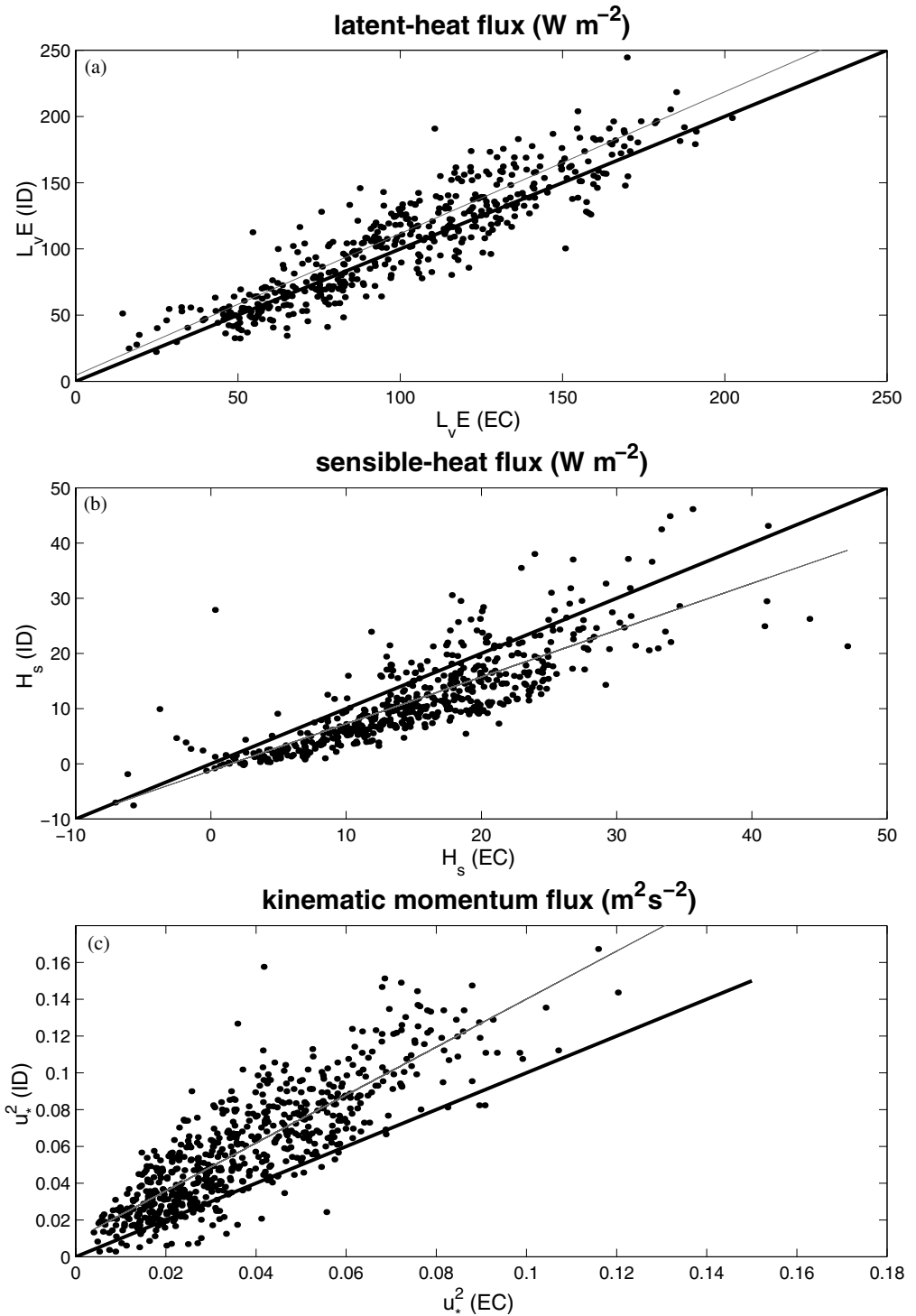


Figure 13. Scatter plots of: (a) latent-heat fluxes, (b) sensible-heat fluxes and (c) momentum fluxes. Values computed by the inertial-dissipation (ID) method are plotted against those computed by the eddy covariance (EC) method. The solid black line is the one-to-one slope and the grey line is the linear best fit.

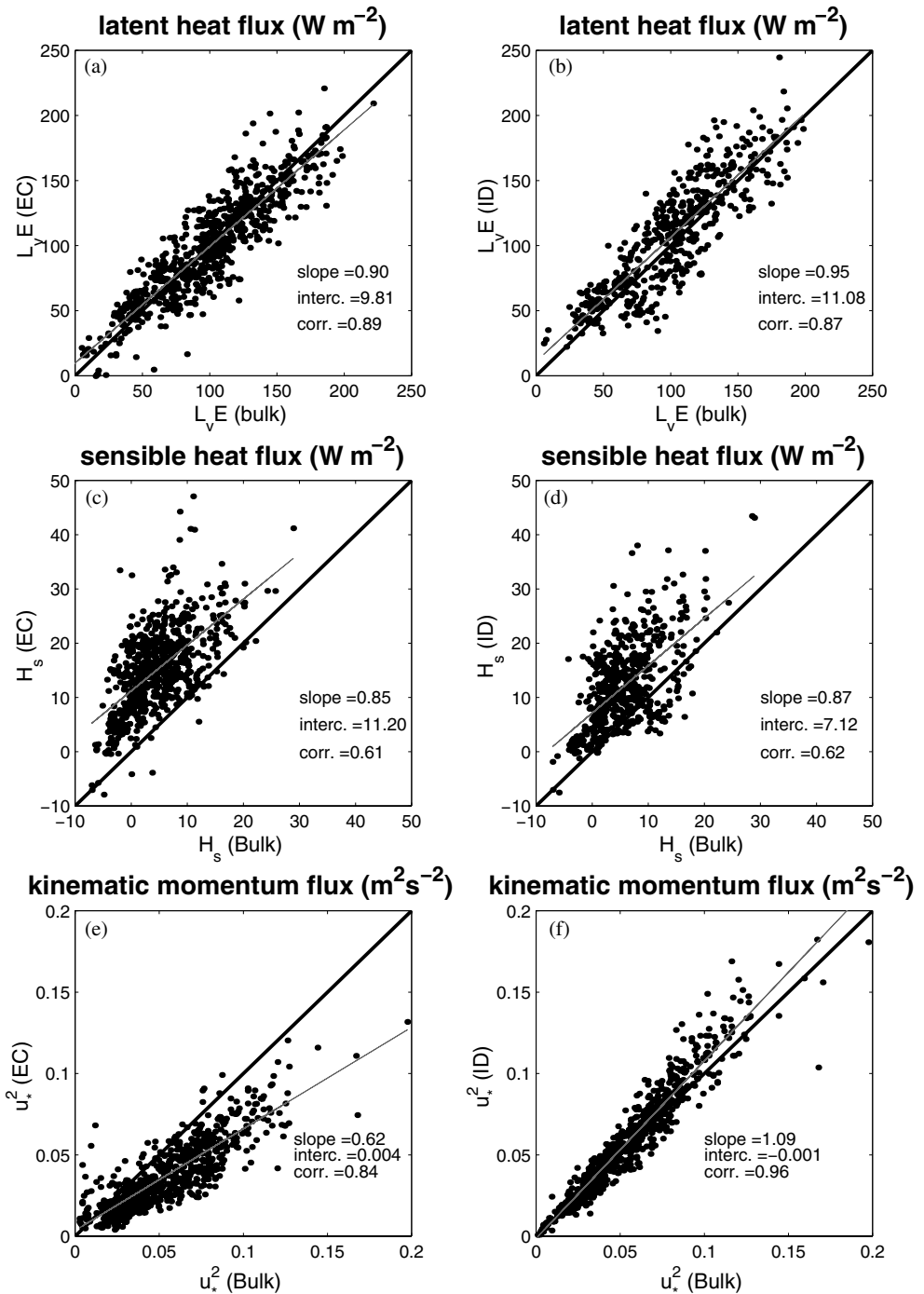


Figure 14. (a) Scatter plot of turbulent latent-heat flux computed by the eddy covariance (EC) method against bulk fluxes computed using the Fairall *et al.* (1996) algorithm (developed for TOGA COARE). The solid black line is the one-to-one slope whereas the solid grey line is the linear fit. The slope, intercept and correlation coefficient for the linear fit are also given. (b) As (a) but computed by the inertial-dissipation (ID) method; (c) and (d), as (a) and (b), but for turbulent sensible-heat flux; (e) and (f), as (a) and (b), but for kinematic momentum flux. See text for further details.

TABLE 5. COMPARISON OF ID AND EC METHODS FOR TURBULENT FLUXES OF MOMENTUM, SENSIBLE HEAT AND HUMIDITY

Comparison $ID = f(EC)$	Number of samples	Correlation r	Linear fit		r.m.s.
			Slope a	Intercept b	
Kinematic momentum flux u_*^2 (m^2s^{-2})	434	0.85	1.31	0.01	0.016
Sensible-heat flux H (W m^{-2})	346	0.82	0.85	-1.23	5.14
Latent-heat flux $L_v E$ (W m^{-2})	311	0.89	1.08	4.62	24.1

See text and Figs. 14 and 15.

the other signals, and they influence the corrections of the measured horizontal wind components. This affects the computation of momentum fluxes using the EC technique and generates the observed bias.

However, another possible cause of such bias can be attributed to swell. For example, Sjöblöm and Smedman (2004) obtained similar results when comparing both methods for the friction velocity, using measurements made on the island of Östergarnsholm. They observed that the mean relative difference between the two methods is about 15% and noticed that this bias is related to swell. On average, the two methods agree well for unstable conditions, but the ID technique gives larger values than the EC method when moving towards neutral conditions, and during stable conditions ID gives significantly larger values than the EC method. They conclude that the ID method works best for near-neutral conditions and high wind speeds, otherwise corrections have to be made depending on the wave age and wind speed.

When comparing time series of sensible-heat flux, a strong variability clearly appears on estimates obtained by the ID technique that is not observed on EC measurements. In addition, since sensible-heat fluxes over the ocean are weak, measuring them accurately remains a difficult task. This results in a high scatter when fluxes estimated by each method are plotted one against the other, as shown in Figs. 13 and 14. For example, in Table 5 which sums up the features of the ID versus EC comparison, the standard error (r.m.s.) is about 5 W m^{-2} , which represents a high degree of scatter when sensible-heat fluxes are weak (from -15 to $+60 \text{ W m}^{-2}$). The correlation coefficient is good ($r = 0.82$) but the regression slope is weak (0.85), indicating that ID fluxes are lower than the EC measurements. This has already been observed during previous experiments (SEMAPHORE, FETCH) during which air temperature fluctuations were recorded using the sonic anemometer. Furthermore, the comparison also shows that bulk estimates are strongly underestimated compared to measurements by both EC and ID (more than 20 W m^{-2} at the beginning of the campaign, and from 9 to 13 August 1999). The low values of bulk sensible-heat flux can be attributed to the use of a sea bulk temperature rather than a skin surface temperature. The difference between the two values can be of importance ($+1 \text{ degC}$) and can therefore considerably modify the flux estimation (Fairall *et al.* 1996).

In order to determine which method was best adapted to compute sensible-heat flux, an example of sonic temperature spectrum is shown in Fig. 15(a). One can see that the sonic temperature signal contains significant levels of noise at high frequencies, and that it does not follow the $-5/3$ power law (i.e. the Kolmogorov theory) in the inertial subrange. This latter aspect tends to limit accurate computation of the sensible-heat flux using the ID method (Larsen *et al.* 1993; Dupuis *et al.* 2003; Weill *et al.* 2003). However, since the sonic thermometer is not contaminated by salt, it can be used to derive turbulent fluxes using the EC method. Figure 15(b) shows a co-spectrum of the sonic temperature

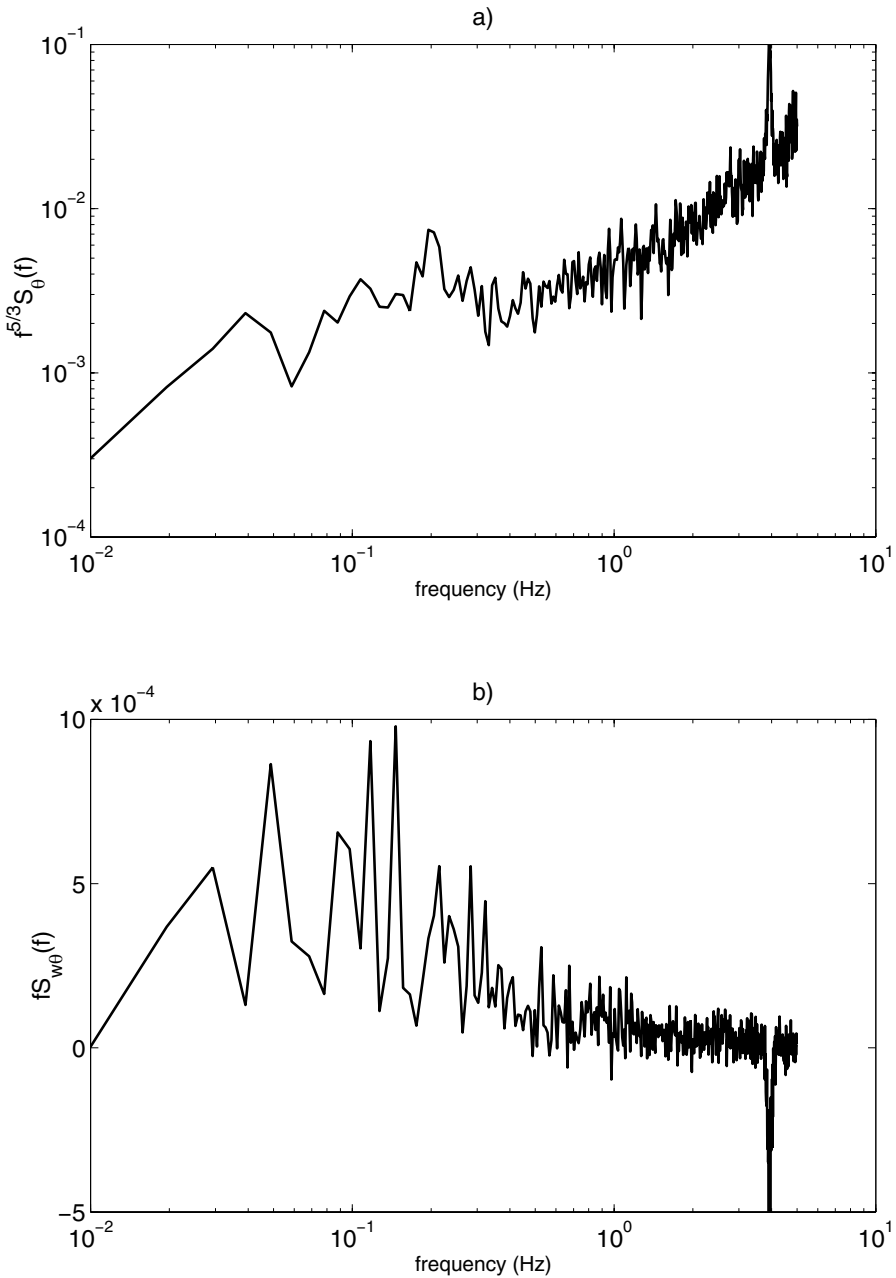


Figure 15. (a) Auto-spectrum of a typical sonic-thermometer signal multiplied by $f^{5/3}$ where f is the frequency; and (b) the co-spectrum (multiplied by f) of the temperature and absolute vertical wind velocity signals. See text for further details.

and vertical wind velocity; it shows a typical shape, with high energy at low frequencies. In this case and on average, heat is carried upward through all frequencies, but at low frequencies the heat flux co-spectrum exhibits more noise. Nevertheless, from spectral considerations the EC method seems to be more appropriate for estimating the sensible-heat flux from ship platforms.

In Fig. 13, it can be seen that latent-heat fluxes reconcile both flux measurement methods, since good agreement is obtained between latent-heat estimates; the regression slope is 1.08 and the scatter is about 24 W m^{-2} . In addition, the latent-heat fluxes computed using the Fairall *et al.* (1996) algorithm are also of the same order of magnitude (see Fig. 14) as the EC and ID fluxes, with high correlation coefficients ($r > 0.85$ in both cases). Again, in order to compare the two methods for estimates of the latent-heat fluxes, we present an example of a specific-humidity spectrum and a co-spectrum of the specific humidity and vertical velocity (Fig. 16). The spectrum of the specific-humidity signal presents a standard shape with a $-5/3$ power law in the inertial subrange. The $\langle wq \rangle$ co-spectrum also exhibits a usual form with higher energy at lower frequencies. Analysis of the spectral information tends to validate the EC method although the uncorrected EC fluxes are slightly higher than the corrected ID data. If we compare these results to bulk estimates (Fig. 14), we see that the EC fluxes are underestimated at low values, whereas they remain in the same range of magnitude as the two other kinds of fluxes at greater values. Actually, this can be explained by increased uncertainties in the EC methods at low wind speeds, for which large eddies are undersampled.

The comparison between the ID and EC methods for computing fluxes for use on board RVs can be summarized as follows:

- Due to the lack of high-frequency information regarding the horizontal motions of the ship, the momentum fluxes computed by the EC technique are doubtful. Thus, the ID method seems to be better adapted to estimate the momentum flux aboard ships.
- From spectral analyses, we deduce that the sensible-heat fluxes derived by EC are of better quality than those obtained by ID method. Consequently, the EC method was chosen to estimate bulk parametrization of C_{Hn} .
- EC and ID techniques show good agreement in latent-heat fluxes; however, since it was only possible to apply corrections for airflow distortion to the ID fluxes, water-vapour fluxes derived by the ID method were used to establish improved parametrizations of C_{En} .

(b) Flux parametrizations and discussion

Figure 17(a) shows that C_{Dn} increases with neutral wind speed. Mean values of C_{Dn} computed over wind speed bins of 1 m s^{-1} are also plotted on this figure and the standard deviations within each bin are represented by error-bars. The dependence of C_{Dn} on U_{10n} is almost linear. The following parametrization is obtained for $4 \text{ m s}^{-1} < U_{10n} < 11 \text{ m s}^{-1}$: $10^3 C_{D10n} = (0.084U_{10n} + 0.548) \pm 0.213$.

The behaviour of the drag coefficient for $U_{10n} < 4 \text{ m s}^{-1}$ is not well characterized, but preliminary indications suggest it increases with decreasing wind velocities (not shown here). Yelland and Taylor (1996) and Fairall *et al.* (1996) observe the same tendency; however, the former observe that at low wind speeds the measurement height of the data (18 m) could have been above the surface layer, whereas the latter suggest that this rise of C_{Dn} is due to the collapse of the usual assumptions underlying the ID method (e.g. Taylor's hypothesis is no longer valid) and to the impact of boundary-layer convection (gustiness).

Although the data were measured over open ocean, this parametrization does not agree with that of Smith (1980) and, more recently, that of Dupuis *et al.* (2003) for the FETCH experiment in the Mediterranean sea. The strong dependence on the neutral wind speed could be attributed to the sea state and wave age. For example, the proposed parametrization is similar to those of the HEXOS dataset for mature and

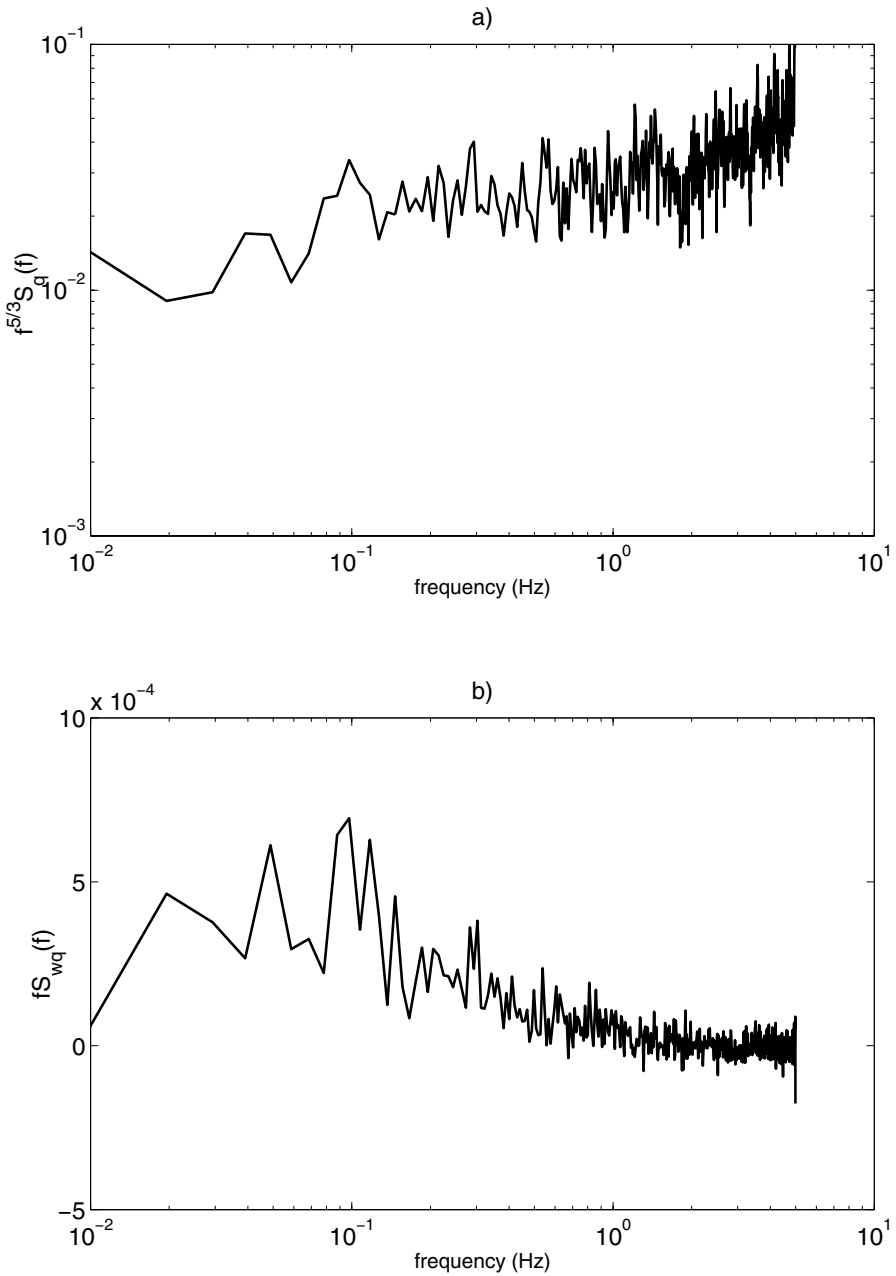


Figure 16. As Fig. 15 but for the specific humidity derived from the refractometer: (a) typical weighted spectrum of the specific humidity, and (b) the cospectrum of the humidity and vertical wind velocity.

fully developed seas. Since EQUALANT99 took place in the Atlantic equatorial large basin, where one would expect long waves and mature or fully developed seas, such agreement is not surprising. However, the HEXOS results provide support for a strong wave-age dependence of the drag coefficient compared to studies from Donelan *et al.* (1997) and Drennan *et al.* (1999). Taylor and Yelland (2001) also observed that the effect of swell in the open ocean introduces scatter into observed C_{Dn} to U_{10n} relationships.

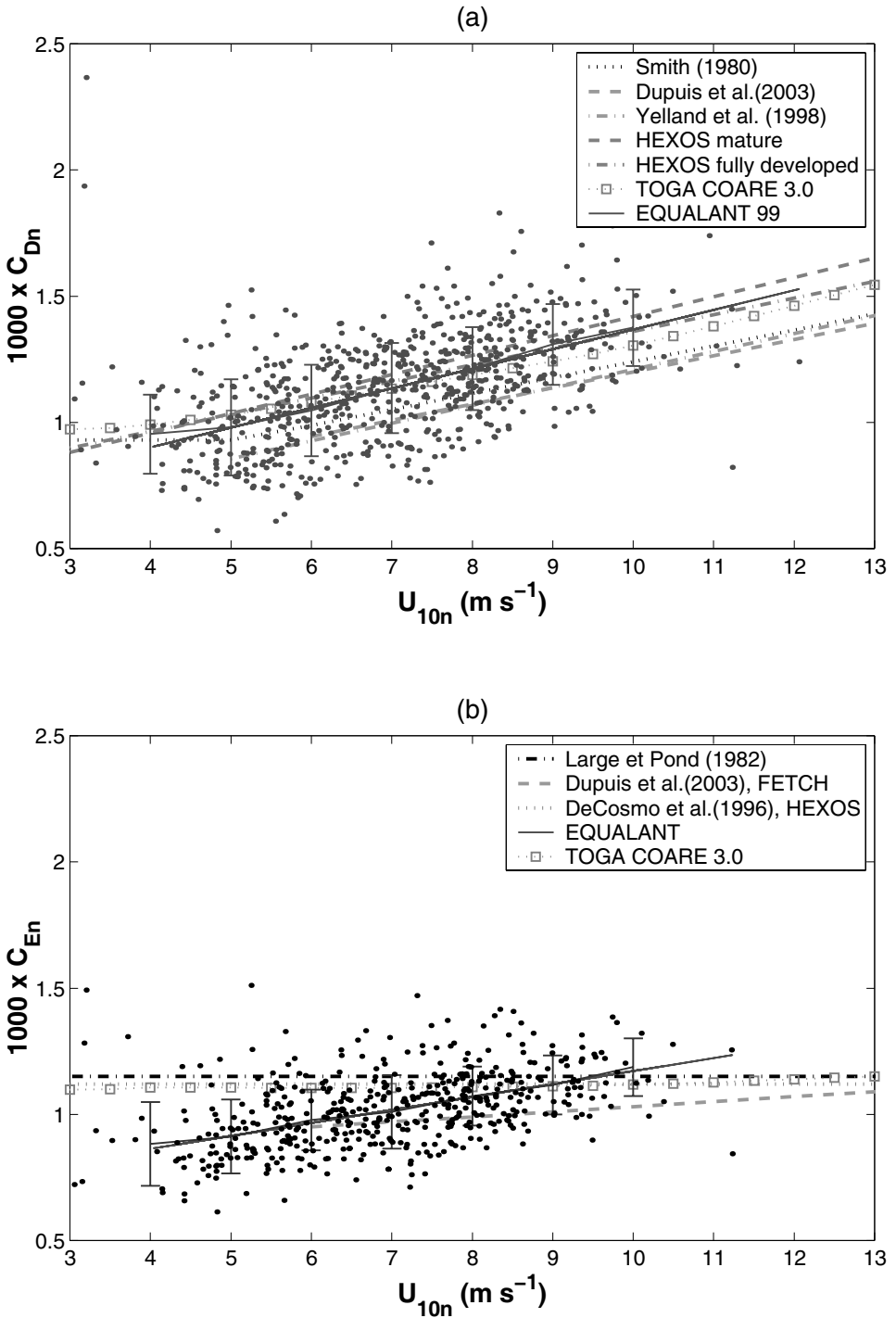


Figure 17. (a) Neutral drag coefficients, C_{Dn} , as a function of the neutral wind speed at 10 m, U_{10n} ; the dots correspond to 30-minute samples, and the solid straight line represents the deduced parametrization. The solid line with error-bars represents values averaged over wind speed bins of 1 m s^{-1} . The parametrizations are as proposed by Smith (1980), Yelland *et al.* (1998) and Dupuis *et al.* (2003); HEXOS and TOGA COARE results are also plotted. (b) As (a) but for the neutral exchange coefficient for moisture, C_{En} , and including the parametrizations of Large and Pond (1982) and DeCosmo *et al.* (1996). See text for further details.

TABLE 6. COMPARISON OF FEATURES OF THE EQUALANT99 DATASET WITH OTHER PARAMETRIZATIONS OF C_{Dn} ($\times 10^3$)

	Slope	Intercept	Correlation coefficient	Range of U_{10n} ($m s^{-1}$)	Number of samples	Angle of azimuth
EQUALANT99	0.084	0.548	0.58	4–13	680	+/-30°
Smith (1980)	0.063	0.61	0.70	6–22	63	–
Yelland <i>et al.</i> (1998)	0.071	0.50	0.80	6–25	1111	+/-10°
Dupuis <i>et al.</i> (2003)	0.064	0.56	0.56	6–19	394	+/-30°

C_{Dn} is the drag coefficient and U_{10n} is the 10 m wind speed, both in neutral stability conditions. See text for other details.

For high wind speeds, the effect of swell was to decrease mean C_{Dn} compared to pure wind sea cases. Unfortunately, no measurements of the sea state were carried out during EQUALANT99 and the same dependence of the drag coefficient as the HEXOS relation cannot be verified. However, an encouraging result is that the EQUALANT99 relation compares well with the latest version of the TOGA COARE parametrization (TC3.0, Fairall *et al.* 2003); this parametrization is also plotted on Figs. 17(a) and (b). On average, both relations are of the same order of magnitude: the TC3.0 parametrization intercepts the EQUALANT99 parametrization at a neutral wind speed of $7.5 m s^{-1}$, and the former falls within the range of measurement uncertainties of the latter.

The characteristics of the EQUALANT99 dataset and other bulk parametrizations are summed up in Table 6. The correlation coefficient ($r = 0.58$) for this linear regression is quite high since it is obtained for a large number of samples. It is lower than that of Yelland *et al.* (1998) who obtained a very high correlation of 0.8 for a large number of samples (1111), but it is better than those of Smith (1980) and Dupuis *et al.* (2003) who used smaller datasets. This good correlation tends to increase our confidence in the bulk parametrization for EQUALANT99.

The results concerning the neutral exchange coefficient for evaporation are presented in Fig. 17(b). The C_{En} parametrization is obtained by a least-squares linear fit. For neutral wind speeds varying between 4 and $10 m s^{-1}$, the formula is:

$$10^3 C_{E10n} = (0.055U_{10n} + 0.63) \pm 0.1324.$$

This regression line, computed using the whole dataset, is similar to the mean values of C_{En} computed using wind speed bins of $1 m s^{-1}$. The accuracy of the linear fit validates the assumption of the dependency of C_{En} on the neutral 10 m wind speed. Furthermore, the C_{En} values do not show a large scatter: the average standard deviation is 0.13×10^{-3} for 468 samples. This characteristic has already been noted in the FETCH dataset (Dupuis *et al.* 2003) and can be attributed to the accuracy of the measurements obtained from the refractometer. The airflow distortion corrections also reduce the scatter of C_{En} versus U_{10n} (see previous section). The correlation coefficient for the bulk parametrization is 0.53, which is an excellent result for evaporation exchange coefficients. During the FETCH experiment, Dupuis *et al.* (2003) obtained a correlation of 0.22 for 290 samples. Unlike many previous studies, they also observed a linear increase of C_{En} with U_{10n} , although the slope was lower than that for the EQUALANT99 dataset. The mean value of C_{En} for the whole dataset is 1.02×10^{-3} , which compares well with the values proposed by Large and Pond (1982), Anderson (1993) and De Cosmo *et al.* (1996).

The scatter of C_{Hn} (r.m.s. = 0.374×10^{-3}) presented in Fig. 18 is greater than for the other coefficients. Low air-sea temperature differences and hence low fluxes are partly responsible for this high scatter. For example, during EQUALANT99 the

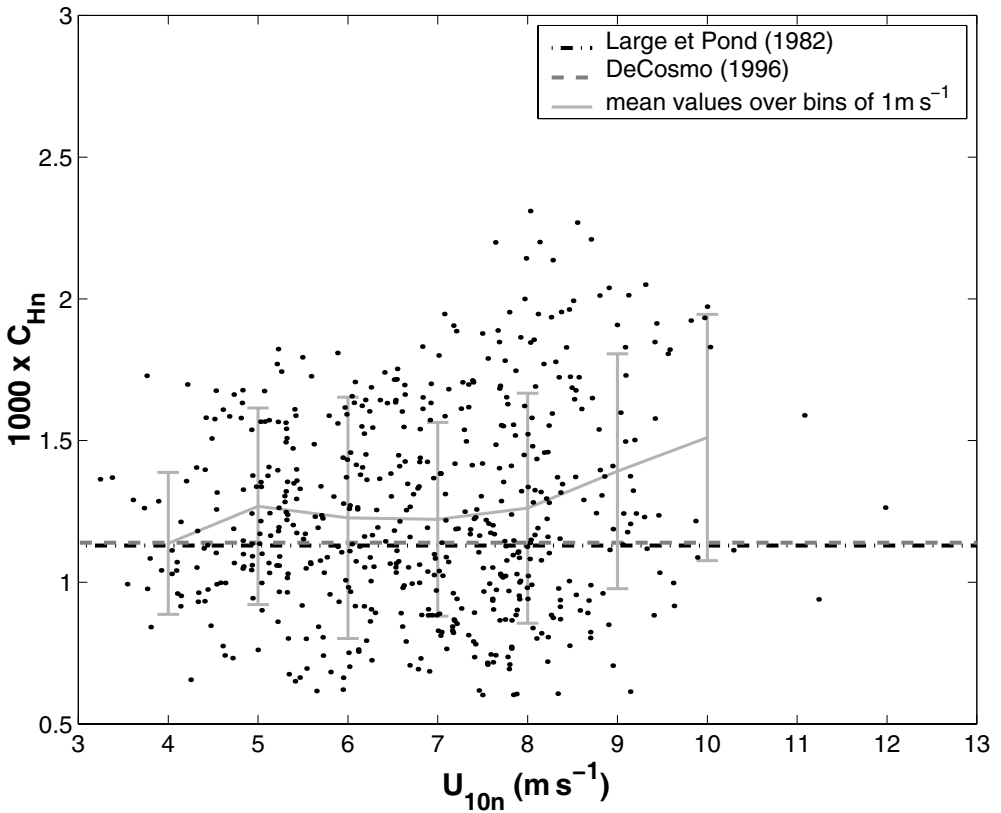


Figure 18. The exchange coefficient for temperature, C_{Hn} , as a function of the neutral wind speed at 10 m, U_{10n} . The dots correspond to 30-minute samples. The solid line with error-bars represents the values averaged over wind speed bins of 1 m s^{-1} . The parametrizations proposed by Large and Pond (1982) and DeCosmo *et al.* (1996) are also plotted.

sensible-heat flux varied between -25 and $+50 \text{ W m}^{-2}$. It remains difficult to find accurately a dependence of C_{Hn} on wind speed. We intended to establish a linear fit corresponding to the mean C_{Hn} curve, but the correlation for such a relation was weak; therefore, the mean value over the whole wind speed range was chosen: $10^3 \times C_{Hn} = 1.3 \pm 0.37$, for U_{10n} varying between 4 and 11 m s^{-1} .

This mean value is larger than the value of 1.13×10^{-3} found by Large and Pond (1982) for unstable atmospheric conditions, and that proposed by DeCosmo *et al.* (1996) for the HEXOS experiment. Actually, although the ID method proved to be less suited to derive parametrizations of C_{Hn} , sensible-heat fluxes computed by both the EC and ID techniques show higher values than bulk estimates. In addition, due to uncertainties associated with the mean values of the transfer coefficient for temperature, the EQUALANT99 relation remains in the range of previous parametrizations. Empirical laws for C_{Hn} have always been difficult to determine due to weak heat fluxes above the sea.

5. CONCLUSIONS

The objectives of this study concern the estimation and the parametrization of turbulent air–sea fluxes for the equatorial Atlantic area using the EQUALANT99 dataset.

Both EC and ID methods were applied to data obtained on board the RV *La Thalassa*, and used to derive fluxes of momentum, sensible and latent heat. The main improvement proposed by this paper is the correction for airflow distortion, based on physical simulations in a water channel, and the determination of accurate parametrizations of turbulent fluxes from a significant body of statistics.

This analysis of the EQUALANT99 dataset fits in with the framework of the ALBATROS database (Weill *et al.* 2003); this allows us to draw some conclusions about the instrumentation used during EQUALANT99 and the methodology used in airflow corrections.

Firstly, a comparison of the EC, ID and bulk calculation techniques points out the drawbacks of each method in the case of the EQUALANT99 experimental set-up. For example, the ID method provides good quality momentum and evaporation fluxes, whereas the sensible-heat flux derived from this technique is less reliable. Spectral analysis allowed us to conclude that the underestimation observed on EC momentum fluxes was probably due a lack of information on the ship's horizontal velocities. A high degree of scatter was observed among heat fluxes computed by the ID method when a sonic anemometer was used to measure fluctuations of air temperature. According to Weill *et al.* (2003) and Dupuis *et al.* (2003) the utility of this instrument for determining air temperatures is limited, due to spikes in the spectra at high frequencies and noise in the inertial subrange. As shown on the example of a typical spectrum of a sonic temperature signal, we observed similar behaviour during EQUALANT99. Nevertheless, this does not seem to affect co-spectrum of temperature and vertical velocities at lower frequencies.

To account for airflow distortion, physical simulations were performed in a water channel. The near-neutral conditions encountered during EQUALANT99 were reproduced to provide the estimate of wind speed errors. Since the detailed structure of the mast was reproduced in the model, it was possible to quantify the impact of the mast and the ship structure on the stream flow; according to Butet (2001), the mast shape with its instrumental set-up has a dominant effect when compared to the ship hull. The originality of this study is that the correction for the wind speed is evaluated as a function of the relative wind azimuth and incidence angles and is applied at 1 Hz. The measurement height must also be corrected for the uplift Δh in bulk formulae. The full correction (wind speed and airflow uplift) had a significant effect on the neutral exchange coefficients: we noticed a decrease of 20% in C_{Dn} and about 10% in C_{En} . Furthermore, the scatter of neutral coefficients as a function of U_{10n} is substantially reduced after the corrections for airflow distortion have been made. Thus the correction resulted in a significant improvement in the bulk parametrizations.

The neutral drag coefficient is much more dependent on the wind speed than typical results over open ocean (Smith 1980; Yelland *et al.* 1998; Dupuis *et al.* 2003). However, good agreement is found with the HEXOS results for mature and fully developed seas. These results should not be surprising: given that EQUALANT99 took place in the large Atlantic equatorial basin, we would expect long waves and strong swell during this experiment. The slight linear dependence observed in C_{En} is more unusual, although this too has been previously observed by Dupuis *et al.* (2003). This strong dependence on the wind speed can be attributed to the method applied to account for airflow distortion. Compared to previous studies which used a single correction per flux sample, in this case corrections were applied at 1 Hz in order to include the ship's position with respect to the sea surface. The neutral coefficient for heat transfer does not show particular dependence on the neutral wind speed; its mean value is higher than previous studies but remains in the range of uncertainties. In the future we hope to extend this study by

using the POMME dataset; that will provide a larger number of samples from a range of different conditions including larger air–sea temperature differences.

ACKNOWLEDGEMENTS

The EQUALANT99 experiment was funded by the Institut de Recherche pour le développement, IFREMER and CNRS/INSU. It was also supported by PNEDC (Programme National d'Etude de la Dynamique et du Climat) and by PNTS. The authors would like to express their gratitude to all the technical and scientific teams who were involved in this experiment and to all the individuals who were in charge of data acquisition. We are also grateful to the TRAMM team (CNRM) for their work of data processing, and to T. Douffet for his involvement in the cruise. We wish to thank all the officers and crew members who took part in the cruise of EQUALANT99 and ensured its success, and C. Andrié, Y. Gouriou and B. Bourlès for organizing this campaign. We are grateful to Hélène Dupuis for her helpful comments and critical remarks about this study. Especially, we would like to thank Dr J. Salmond who read this paper and corrected English formulations. Also we thank the two anonymous reviewers for their conscientious work who contributed to greatly improve our manuscript.

REFERENCES

- Ancil, F., Donelan, M. A. and Graber, H. C. 1994 Eddy-correlation measurements of air–sea fluxes from a discus buoy. *J. Atmos. Oceanic Technol.*, **11**, 1144–1150
- Anderson, R. J. 1993 A study of wind stress and heat flux over the open ocean by the inertial dissipation method. *J. Phys. Oceanogr.*, **23**, 2153–2161
- Blanc, T. V. 1986 'Superstructure flow distortion corrections for wind speed and direction measurements made from Tarawa Class (LHA1–LHA5) ships'. NRL report 9005, Naval Research Laboratory, Washington, DC, USA
- 1987 'Superstructure flow distortion corrections for wind speed and direction measurements made from Virginia Class (CGN38–CGN41) ships'. NRL report 9026, Naval Research Laboratory, Washington, DC, USA
- Brut, A., Butet, A., Planton, S., Durand, P. and Caniaux, G. 2002 'Influence of airflow distortion on air–sea flux measurements aboard research vessels: Results of physical simulations applied to the EQUALANT99 experiment'. In Proceedings of the 15th symposium on boundary layers and turbulence, 15–19 July 2002, Wageningen, the Netherlands. American Meteorological Society, Boston, USA
- Brut, A., Legain, D., Durand, P. and Laville, P. 2004 A relaxed eddy accumulator for surface flux measurements on ground-based platforms and aboard research vessels. *J. Atmos. Oceanic Technol.*, **21**, 411–427
- Butet, A. 2001 'Simulation du vent autour du N.O. *La Thalassa*'. Note de centre No. 23, CNRM, GMEI, Météo-France, Toulouse, France
- Castro, I. P. and Robins, A. G. 1977 The flow around a surface-mounted cube in uniform and turbulent streams. *J. Fluid Mech.*, **79**, 307–335
- Charnock, H. 1955 Wind stress on a water surface. *Q. J. R. Meteorol. Soc.*, **81**, 639–640
- DeCosmo, J., Katsaros, K. B., Smith, S. D., Anderson, R. J., Oost, W. A., Bumke, K. and Chadwick, H. 1996 Air–sea exchange of sensible heat and water vapor: The HEXOS results. *J. Geophys. Res.*, **101**, 12001–12016
- Delahaye, J. Y., Guérin, C., Vinson, J. P., Dupuis, H., Weill, A., Branger, H., Eymard, L., Lavernat, J. and Lachaud, G. 2001 A new shipborne microwave refractometer for estimating the evaporation flux at the sea surface. *J. Atmos. Oceanic Technol.*, **18**, 459–475
- Donelan, M., Dobson, F., Smith, S. D. and Anderson, R. A. 1993 On the dependence of sea surface roughness on wave development. *J. Phys. Oceanogr.*, **23**, 2143–2149

- Donelan, M. A., Drennan, W. M. and Katsaros, K. B. 1997 The air-sea momentum flux in conditions of wind sea and swell. *J. Phys. Oceanogr.*, **27**(10), 2087-2099
- Drennan, W. M., Graber, H. C. and Donelan, M. A. 1999 Evidence for the effects of swell and unsteady winds on marine wind stress. *J. Phys. Oceanogr.*, **29**, 1853-1864
- Drennan, W. M., Graber, H. C., Hauser, D. and Quentin, C. 2003 On the wave age dependence of wind stress over pure wind seas. *J. Geophys. Res.*, **108**(C11), doi: 10.1029/2000JC000715
- Dugan, J. P., Panichas, S. L. and Dimarco, R. L. 1991 Decontamination of wind measurements from buoys subject to motions in seaways. *J. Atmos. Oceanic Technol.*, **8**, 85-95
- Dupuis, H., Taylor, P., Weill, A. and Katsaros, K. 1997 Inertial dissipation method applied to derive turbulent fluxes over the ocean during the Surface of the Ocean, Fluxes and Interactions with the Atmosphere/Atlantic Stratocumulus Transition Experiment (SOFIA/ASTEX) and Structures des Echanges Mer-Atmosphere, Proprietes des Heterogeneites Oceaniques: Recherche Experimentale (SEMAPHORE) experiments with low to moderate wind speeds. *J. Geophys. Res.*, **102**(C9), 21115-21129
- Dupuis, H., Guérin, C., Hauser, D., Weill, A., Nacass, P., Drennan, W., Cloché, S. and Graber, H. 2003 Impact of flow distortion corrections on turbulent fluxes estimated by the inertial dissipation method during the FETCH experiment on R/V *L'Atalante*. *J. Geophys. Res.*, **108**(C3), 8064, doi: 10.1029/2001JC001075
- Dyer, A. J. 1974 A review of flux profile relationships. *Boundary Layer Meteorol.*, **7**, 363-372
- Edson, J. B. and Fairall, C. W. 1994 Spray droplet modeling. I: Lagrangian model simulation of the turbulent transport of evaporating droplets. *J. Geophys. Res.*, **99**, 25295-25311
- 1998 Similarity relationships in the marine atmospheric surface layer for terms in the TKE and scalar variance budgets. *J. Atmos. Sci.*, **55**, 2311-2328
- Edson, J. B., Fairall, C. W., Mestayer, P. G. and Larsen, S. E. 1991 A study of the inertial-dissipation method for computing air-sea fluxes. *J. Geophys. Res.*, **96**(C6), 10689-10711
- Edson, J. B., Hinton, A. A., Prada, K. E., Hare, J. E. and Fairall, C. W. 1998 Direct covariance flux estimates from mobile platforms at sea. *J. Atmos. Oceanic Technol.*, **15**, 547-562
- Eymard, L., Planton, S., Durand, P., Camus, Y., Le Traon, P. Y., Prieur, L., Weill, A., Hauser, D., Le Square, B., Rolland, J., Pelon, J., Baudin, F., Bénéch, B., Brenguier, J. L., Caniaux, G., De Mey, P., Dombrowski, E., Druilhet, A., Dupuis, H., Ferret, B., Flamant, C., Flamant, P., Hernandez, F., Jourdan, D., Katsaros, K., Lambert, D., Lefèvre, J. M., Le Borgne, P., Marsouin, A., Roquet, H., Tournadre, J., Trouillet, V. and Zakardjian, B. 1996 Study of the air-sea interactions at the mesoscale: The SEMAPHORE experiment. *Annales Geophysicae*, **14**, 986-1015
- Eymard, L., Caniaux, G., Dupuis, H., Prieur, L., Giordani, H., Troadec, R., Bourras, D., Guérin, C., Le Borgne, P., Brisson, A. and Marsouin, A. 1999 Surface fluxes in the North Atlantic current during the CATCH/FASTEX experiment. *Q. J. R. Meteorol. Soc.*, **125**, 3563-3599
- Fairall, C. W. and Larsen, S. E. 1986 Inertial dissipation methods and turbulent fluxes at the air ocean interface. *Boundary Layer Meteorol.*, **34**, 287-301
- Fairall, C. W., Bradley, E. F., Rogers, D. P., Edson, J. B. and Young, G. S. 1996 Bulk parameterization of air-sea fluxes for TOGA-COARE. *J. Geophys. Res.*, **101**, 3747-3764
- Fairall, C. W., Bradley, E. F., Hare, J. E., Grachev, A. A. and Edson, J. B. 2003 Bulk parameterization of air-sea fluxes: Updates and verification for the TOGA COARE algorithm. *J. Climate*, **16**(4), 571-591
- Fujitani, T. 1981 Direct measurement of turbulent fluxes over the sea during AMTEX. *Pap. Meteorol. Geophys.*, **32**, 119-134

- Geernaert, G. L. 1990 Bulk parameterizations for the wind stress and heat fluxes. Pp. 91–172 in *Surface waves and fluxes*. Vol. I. Eds. G. L. Geernaert and W. J. Plant. Kluwer, Dordrecht, the Netherlands
- Gouriou, Y., Andrié, C., Bouflès, B., Freudenthal, S., Arnault, S., Aman, A., Eldin, G., du Penhoat, Y., Baurand, F., Gallois, F. and Chuchla, R. 2001 Deep circulation in the equatorial Atlantic Ocean. *Geophys. Res. Lett.*, **28**, 819–822
- Grachev, A. A. and Fairall, C. W. 2001 Upward momentum transfer in the marine boundary layer. *J. Phys. Oceanogr.*, **31**, 1698–1711
- Hauser, D., Branger, H., Bouffières-Cloch e, S., Despi au, S., Drennan, W., Dupuis, H., Durand, P., Durieu de Madron, X., Estournel, C., Eymard, L., Flamant, C., Graber, H., Gu erin, C., Kahma, K., Lachaud, G., Lef evre, J. M., Pelon, J., Pettersen, H., Pignat, B., Queff eulou, P., T aille, D., Tournadre, J. and Weill, A. 2003 The FETCH experiment: an overview. *J. Geophys. Res.*, **108**(C3), 8053, doi: 10.1029/2001JC001202,2003
- Henjes, K. 1998 Justification of the inertial dissipation technique in anisotropic mean flow. *Boundary-Layer Meteorol.*, **88**(2), 161–180
- Joly, A., Jorgensen, D., Shapiro, M. A., Thorpe, A. J., Bessemoulin, P., Browning, K. A., Cammas, J. P., Clough, S. A., Emanuel, K. A., Eymard, L., Gall, R., Hildebrand, P. H., Langland, R. H., Lema tre, Y., Lynch, P., Moore, J. A., Persson, P. O., Snyder, C. and Wakimoto, R. M. 1997 Definition of the Fronts and Atlantic Storm-track Experiment (FASTEX). *Bull. Am. Meteorol. Soc.*, **78**(4), 1917–1940
- Kaimal, J. C. and Gaynor, J. E. 1991 Another look at sonic thermometry. *Boundary-Layer Meteorol.*, **56**, 401–410
- Kaimal, J. C., Wyngaard, J. C., Izumi, Y. and Cot e, O. R. 1972 Spectral characteristics of surface-layer turbulence. *Q. J. R. Meteorol. Soc.*, **98**, 563–589
- Katsaros, K. B., Donelan, M. A. and Drennan, W. M. 1993 Flux measurements from a swath ship in Swade. *J. Mar. Systems*, **4**, 117–132
- Komen, G. J., Janssen, P. A. E. M., Makin, V. and Oost, W. A. 1998 On the sea state dependence of the Charnock parameter. *The Global Atmos. and Ocean System*, **5**, 367–388
- Kristensen, L., Mann, J., Oncley, S. P. and Wyngaard, J. C. 1997 How close is close enough when measuring scalar fluxes with displaced sensors? *J. Atmos. Oceanic Technol.*, **14**, 814–821
- Large, W. G. and Pond, S. 1981 Open ocean momentum flux measurements in moderate to strong winds. *J. Phys. Oceanogr.*, **10**, 709–726
- Larsen, S. E. and Gibson, C. H. 1980 Fast-response temperature sensors. Pp. 269–291 in *Air–sea interaction*. Eds. F. Dobson and R. Davis. Plenum Press, New York, USA
- Larsen, S. E., Edson, J. B., Fairall, C. W. and Mestayer, P. G. 1993 Measurements of temperature spectra by a sonic anemometer. *J. Atmos. Oceanic Technol.*, **10**, 345–354
- Larsen, S. E., Nielsen, M., Soerensen, L. L., Smedmann, A. S., Sjoebloom, A., Magnusson, M., Taylor, P. K., Yelland, M., Pascal, R., Clayson, C., Weill, A., Dupuis, H., Westgarth, G., Stickland, T., Koshiek, W. and Oost, W. 2000 ‘AUTOFLUX: an autonomous flux package for measuring the air–sea flux of momentum, heat, water vapour and carbon dioxide’. In Proceedings of euroOCEAN 2000, Hamburg, Germany, 29 August–2 September 2000. European Commission, Brussels, Belgium

- Memery, L., Reverdin, G. and Paillet, J. 2005 The POMME (Programme Océan Multi Disciplinaire Mésos-Echelle) experiment: Subduction, thermocline ventilation and biogeochemical tracer distribution in the north east Atlantic Ocean. Impacts of mesoscale dynamics. *E.O.S.* in press
- Nacass, P. 1999 'Utilisation de la modélisation des écoulements aérodynamiques pour la mesure atmosphérique à bord du navire océanographique L'Atalante'. Note de centre No. 22 CAM, Météo-France, Toulouse, France
- Oost, W. A. 1998 The KNMI HEXMAX stress data reanalysis. *Boundary-Layer Meteorol.*, **86**, 447–468
- Oost, W. A., Fairall, C. W., Edson, J. B., Smith, S. D., Anderson, R. J., Wills, J. A. B., Katsaros, K. B. and DeCosmo, J. 1994 Flow distortion calculations and their application in HEXMAX. *J. Atmos. Oceanic Technol.*, **11**, 366–386
- Pederos, R., Dardier, G., Dupuis, H., Graber, H. C., Drennan, W. M., Weill, A., Guérin, C. and Nacass, P. 2003 Momentum and heat fluxes via the eddy correlation method on the R/V *L'Atalante* and an ASIS buoy. *J. Geophys. Res.*, **108**(C11), 3339, doi: 10.1029/2002JC001449
- Schacher, G. E. and Fairall, C. W. 1976 Use of resistance wires for atmospheric turbulence measurements in the marine environment. *Rev. Sci. Instr.*, **47**, 703–707
- Schmitt, K. F., Friehe, C. A. and Gibson, C. H. 1978 Humidity sensitivity of atmospheric temperature sensors by salt contamination. *J. Phys. Oceanogr.*, **8**, 151–161
- Servain, J., Busalacchi, A. J., McPhaden, M., Moura, A. D., Reverdin, G., Vianna, M. and Zebiak, S. E. 1998 A Pilot Research moored Array in the Tropical Atlantic (PIRATA). *Bull. Am. Meteorol. Soc.*, **79**, 2019–2031
- Sjöblöm, A. and Smedman, A. S. 2004 Comparison between eddy-correlation and inertial dissipation methods in the marine atmospheric surface layer. *Boundary-Layer Meteorol.*, **110**, 141–164
- Smedman, A., Högström, U., Bergström, H., Rutgersson, A., Kahma, K. K. and Pettersson, H. 1999 A case study of air-sea interaction during swell conditions. *J. Geophys. Res.*, **104**, 25833–25851
- Smith, S. D. 1980 Wind stress and heat flux over the ocean in gale force winds. *J. Phys. Oceanogr.*, **10**, 709–726
- Smith, S. D., Fairall, C. W., Geernaert, G. L. and Hasse, L. 1996 Air-sea fluxes: 25 years of progress. *Boundary-Layer Meteorol.*, **78**, 247–290
- Taylor, P. K. and Yelland, M. J. 2000 On the apparent 'imbalance' term in the turbulent kinetic energy budget. *J. Atmos. Oceanic Technol.*, **17**, 82–89
- 2001 The dependence of sea state surface roughness on the height and steepness of the waves. *J. Phys. Oceanogr.*, **31**, 572–590
- Volkov, Y. A. 1970 Turbulent flux of momentum and heat in the atmospheric surface layer over a disturbed surface. *Izv. Acad. Sci. USSR Atmos. Oceanic Phys.*, **6**, 770–774
- Weill, A., Baudin, F., Dupuis, H., Eymard, L., Frangi, J. P., Gerard, E., Durand, P., Bénech, B., Dessens, J., Druilhet, A., Réchou, A., Flamant, P., Elouragini, S., Valentin, R., Sèze, G., Pelon, J., Flamant, C., Brenguier, J. L., Planton, S., Rolland, J., Brisson, A., LeBorgne, P., Marsouin, A., Moreau, T., Katsaros, K., Monis, R., Queuiffeulou, P., Tournadre, J., Taylor, P. K., Kent, E., Pascal, R., Schibler, P., Parol, F., Desclotres, J., Ballois, J. Y., André, M. and Charpentier, M. 1995 SOFIA 1992 experiment during ASTEX. *The Global Atmos. and Ocean System*, **3**, 335–343

- Weill, A., Eymard, L., Caniaux, G., 2003 Toward a better determination of turbulent air–sea fluxes from Hauser, D., Planton, S., Dupuis, H., Brut, A., Gu erin, C., Nacass, P., Butet, A., Cloch e, S., Pedreros, R., Durand, P., Bourras, D., Giordani, H., Lachaud, G. and Bouhours, G. 2003 Toward a better determination of turbulent air–sea fluxes from several experiments. *J. Climate*, **16**, 600–618
- Wucknitz, J. 1979 The influence of anisotropy on stress estimation by the inertial dissipation method. *Boundary-Layer Meteorol.*, **27**, 119–131
- Wyngaard, J. C. 1973 ‘On surface layer turbulence’. Pp. 101–149 in Workshop in micrometeorology. Ed. D. A. Haugen. American Meteorological Society, Boston, USA
- Yelland, M. J. and Taylor, P. K. 1996 Wind stress measurements from the open ocean. *J. Phys. Oceanogr.*, **26**, 541–558
- Yelland, M. J., Taylor, P. K., Consterdine, I. E. and Smith, M. H. 1994 The use of the inertial-dissipation technique for shipboard wind stress determination. *J. Atmos. Oceanic Technol.*, **11**, 1093–1108
- Yelland, M. J., Moat, B. J., Taylor, P. K., Hutchings, R. W. and Cornell, V. C. 1998 Wind stress measurements from the open ocean corrected for airflow distortion by the ship. *J. Phys. Oceanogr.*, **28**, 1511–1525
- Yelland, M. J., Moat, B. J., Pascal, R. W. and Berry, D. I. 2002 CFD model estimates of the airflow over research ships and the impact on momentum flux measurements. *J. Atmos. Oceanic Technol.*, **19**, 1477–1499
- Zeller, K., Zimmerman, G., Hehn, T., Donev, E., Denny, D. and Welker, J. 2001 Analysis of inadvertent microprocessor lag time on eddy covariance results. *J. Appl. Meteorol.*, **40**, 1640–1646